Zeitschrift: IABSE congress report = Rapport du congrès AIPC = IVBH Kongressbericht

Band: 10 (1976)

Rubrik: Theme Va: Structural behavior including hybrid construction

Versuchsergebnisse vorgespannter Stahlträger im elastischen und elastoplastischen Zustand

Results of Tests of Prestressed Steel Beams in Elastic and Elastoplastic State

Résultats d'essais sur des poutres en acier précontraintes, à l'état élastique et élastoplastique

PAVEL FERJENCIK
Dozent, Dipl.-Ing., CSc
Fakultät für Bauwesen der Slowakischen Technischen Hochschule
Bratislava, CSSR

MILOSLAV TOCHACEK
Dipl.-Ing. CSc
Bauinstitut der Tschechischen TU Praha
Praha, CSSR

Ziel der Prüfungen sechs vorgespannter Walzträger war die Ermittlung der wirklichen Wirkung dieser Träger, im elastischen wie auch im elastoplastischen Zustand und der Vergleich der Ergebnisse mit der Theorie /1/. Es waren grundsätzlich diese Gründe für die Wahl der Walzträger: Überprüfung der Theorie an herstellungsmässig einfachen Elementen, die geringe Anschaffungskosten haben, und Überprüfung der Verstärkungsmöglichkeit so wie auch der Tragfähigkeitserhöhung der Walzträger durch vorgespannte hochfeste Zugbänder.

Verwendet wurden Walzträger I PE 30 aus Stahl 11 373 mit 3800 mm Spannweite. Auf der ganzen Spannweitelänge waren die Träger mit einem hochfestem Zugband aus patentierten Drähten 20 Ø P 4,5 mm vorgespannt; das Zugband lief unter dem Trägeruntergurtflansch, parallel mit diesem, Bild 1. Die Träger N 1 bis N 6

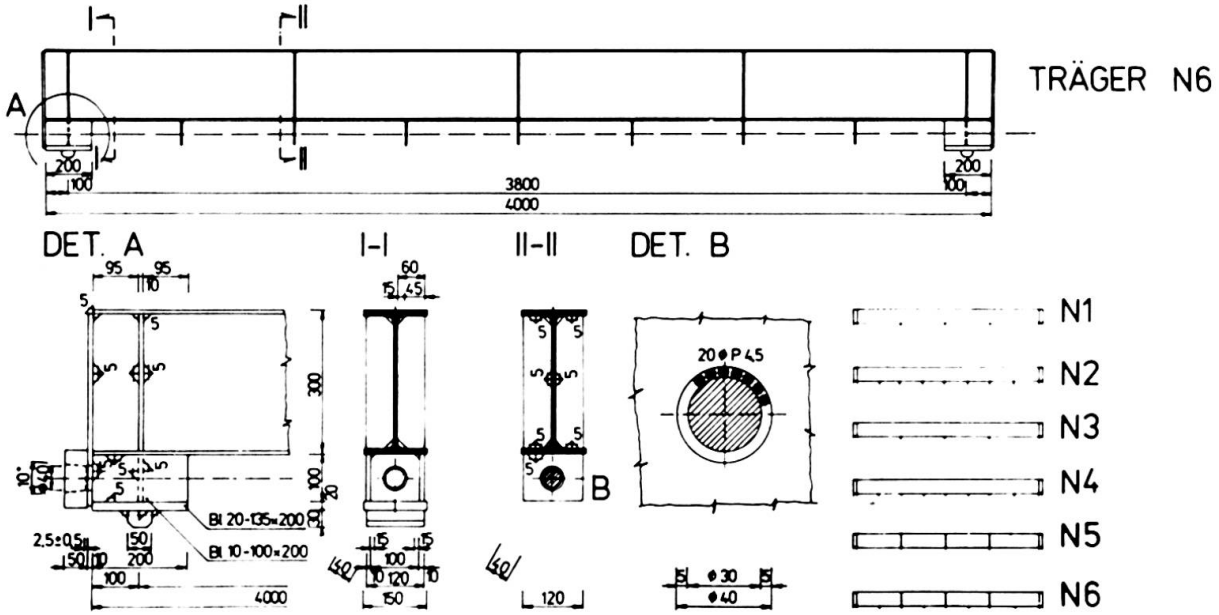

Bild 1. Prüfträger N 1 bis N 6

hatten unterschiedliche Zahlen der Stegdiafragmen, stabilisierenden Diafragmen unter dem Trägeruntergurtflansch und Einlagen im Zugbandinneren.

Die Ansicht der Gesamtanordnung der Prüfung ist am Bild 2 zu sehen. Oben sieht man den stützenden Hilfsträger, unten ist der Prüfträger, zwischen beiden Trägern sind drei Belastungspressen. Die Vorrichtung am Bild 2 rechts sichert die Stabilität der geprüften Konstruktion. Am Bild 3 ist das Zugband vom Ringquerschnitt an der Stelle des stabilisierenden Diafragma mit /Bild 3a/ und ohne /Bild 3b/ der pressenden Einlagen. Die Vorspannpistole /Bild 4/ stützte sich auf den ringförmigen Dynamometer, mit dem die Zugbandkraft kontrolliert wurde.

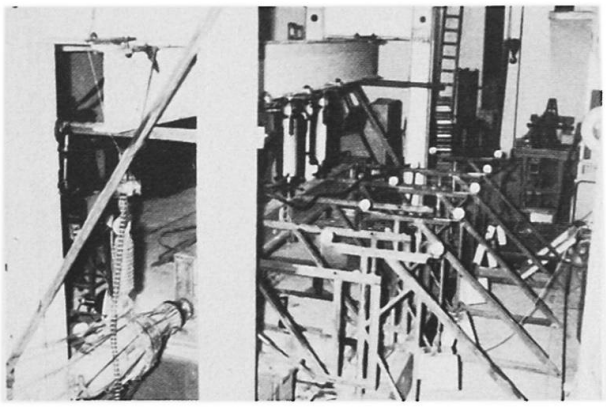

Bild 2.

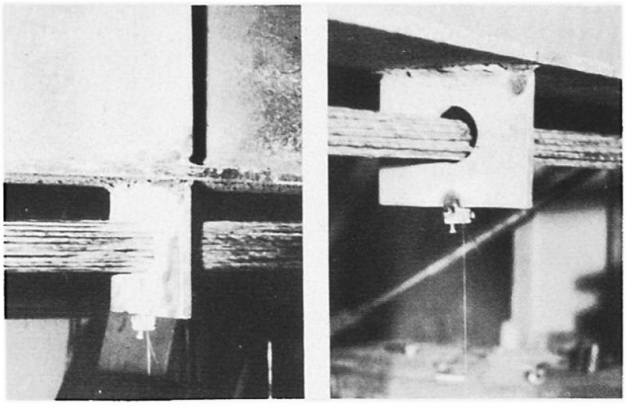

a/ b/

Bild 3.

Die Spannungen im Träger wurden mit 16 Widerstandstensometern gemessen, die 10 cm von der Spannweitemitte des Trägers angeordnet waren. Die Durchbiegungen wurden mittels Durchbiegungsmessern an den Viertelpunkten der Spannweite /unter den Lasten/ gemessen, Bild 5.

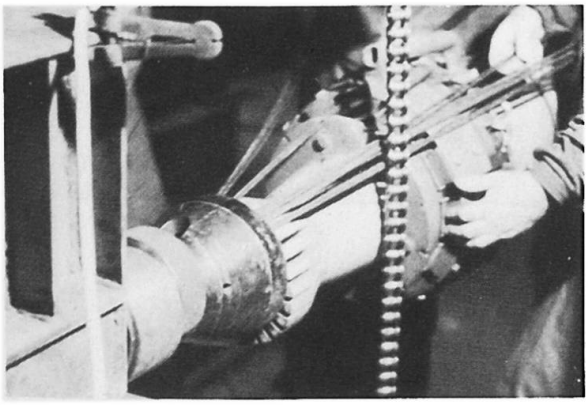

Bild 4.

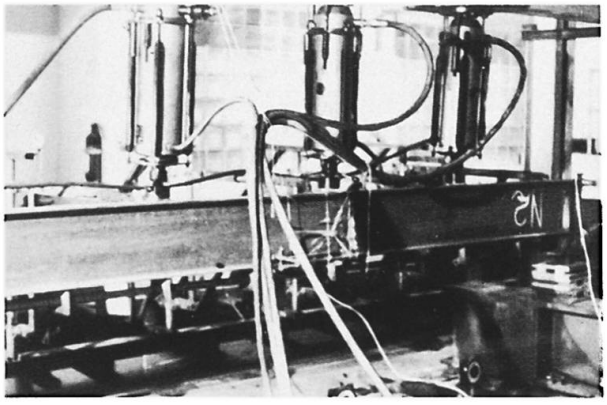

Bild 5.

Kontrolliert wurde auch die Stützensenkung. Bei zwei Trägern wurde die Trägerstabilität mit einer Ergänzungsprüfung gemessen, und zwar bei der Belastung nur durch die Vorspannkraft V: in einem Falle nach Beseitigung aller stabilisierenden Diafragmen /Bild 6/, in zweitem Fall beim Belassen dieser in der Spannweitemitte des Trägers.

Bei den Trägerprüfungen kamen folgende Belastungsstufen zur Geltung: Vorspannkraft V = 0-50-100-150-250-300 kN; lotrechte Lasten P = 0-20-5-40-5-60-5-80-5-90-5-100-110 kN, usw. bis zum Bruch der Konstruktion.

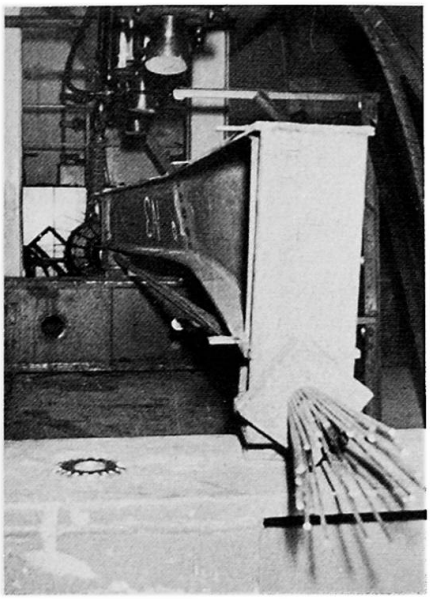

Bild 6. Stabilitätsverlust des Trägers, bei dem die stabilisierenden Diafragmen beseitigt wurden

Die Messergebnisse sind zu Diagrammen verarbeitet, von welchen je eines die Bilder 7 und 8 zeigen. Die erste Diagrammgruppe, die im Bild 7 gezeigt wird, stellt den Verlauf der Normalspannungen in der Trägermitte dar. Der Diagrammtyp im Bild 8 stellt das Anwachsen der verhältnismässigen Verformungen dar /lotrecht aufgetragen/, nachdem sie durch den Elastizitätsmodul multipliziert wurden /im elastischen Bereich also der Normalspannungen σ /in Abhängigkeit vom Anwachsen der Vorspannkraft V /horizontal nach rechts/ und der Belastung P /zurück in der Linksrichtung/. Ähnlich wurden die Messergebnisse der Durchbiegung y verarbeitet, Bild 9.

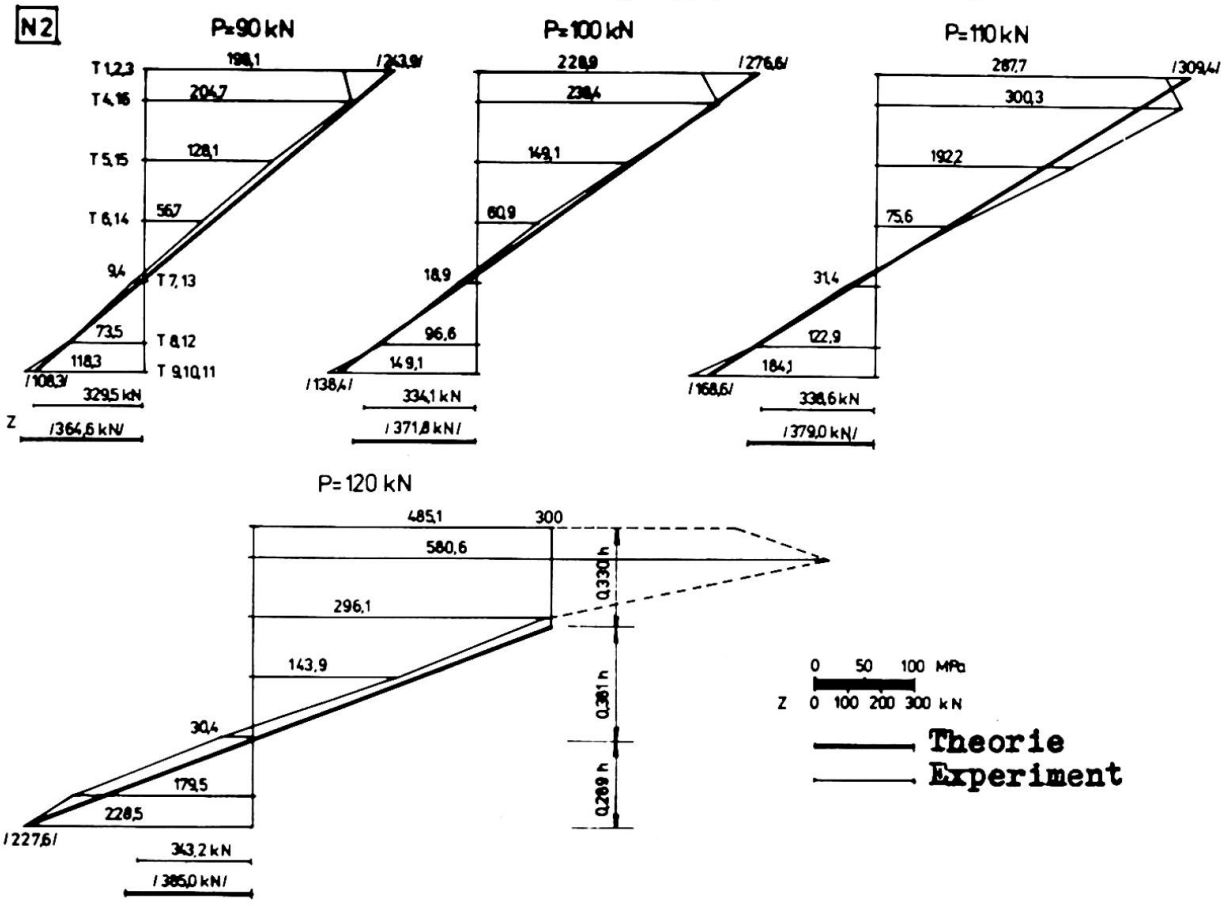

Bild 7. Träger N 2: Normalspannungen in der Mitte der Spannweite bei verschiedener Belastungsgrösse 3xP

Die Prüfungen brachten folgende Erkenntnisse:

Die erwartete Tragfähigkeit vorgespannter Träger im elastischen Zustand /bei der Normfliessgrenze σ_{fl} = 240 MPa grösser als Berechnungsbeanspruchung R = 210 MPa/ war 3x90 kN. Durch den Einfluss noch höherer wirklicher Fliessgrenze $\sigma_{fl} \doteq$ 300 MPa, stieg die theoretische elastische Tragfähigkeit auf cca 3x110 kN. Nach der Norm /2/ berech-

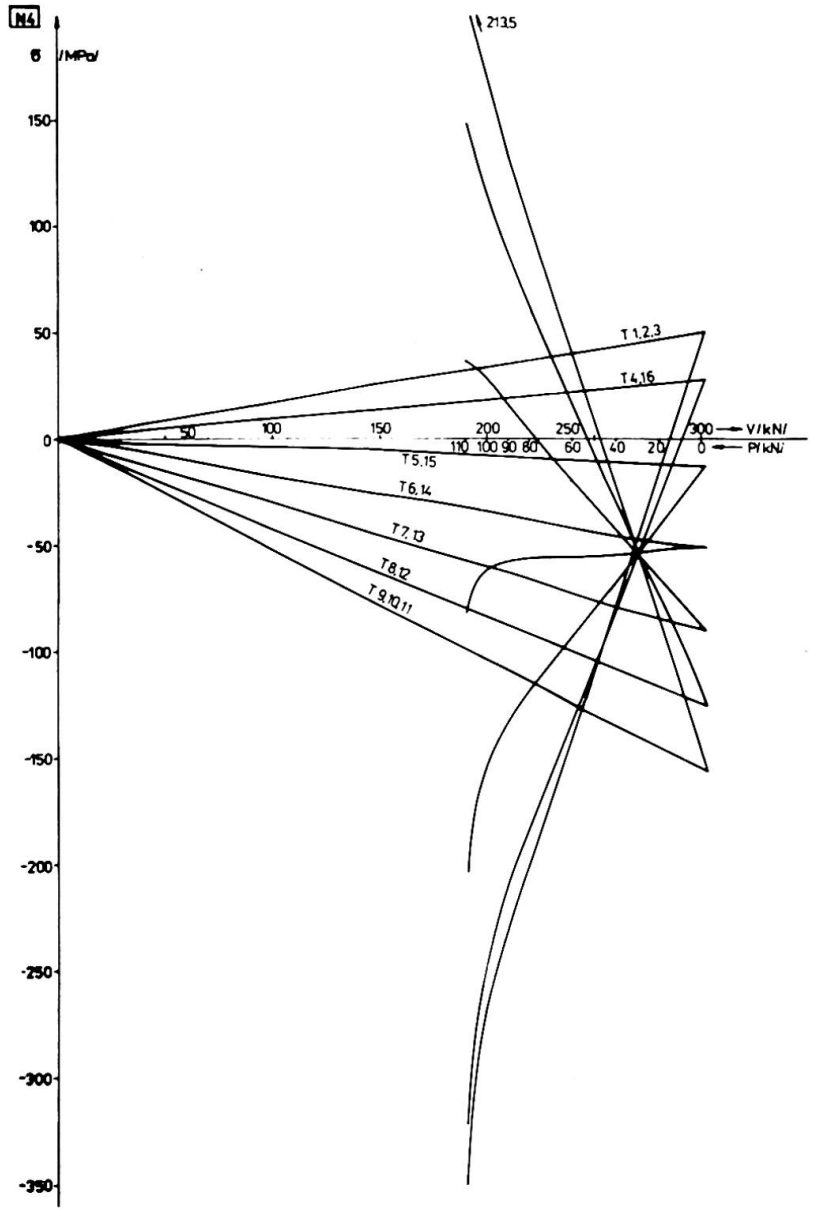

Bild 8. Träger N 4: Spannungsverlauf in Abhängigkeit von der Vorspannung V und Belastung P

net sich bei R = 210 MPa die tragende Last eines nicht vorgespannten Trägers I PE 30 mit 3x61,6 kN. In den ersten vier Trägern wurde eine hohe Tragfähigkeit erreicht, cca die doppelte des nach /2/ berechneten nicht vorgespannten Trägers. Bei den letzten zwei Trägern kam es zur Verringerung der Tragfähigkeit infolge Kippens; die Stützvorrichtung konnte den Obergurt nicht halten - auch so erreichte man eine um die Hälfte grössere Tragfähigkeit als beim nicht vorgespannten, nach /2/ berechneten, Träger.

Tensometrische Messungen zeigten eine sehr gute bis gute Übereinstimmung der Theorie und der Experimente. Es zeigte sich, dass mit den Vorkehrungen, die die Stabilität der Trägerdruckteile sichern, plastische Bereiche hervorgerufen werden können.

Die Durchbiegungsmessungen brachten folgende Erkenntnisse:

- Solange nur die Vorspannkraft wirkte, bestand eine sehr gute Übereinstimmung der theoretischen und gemessenen Durchbiegungen.

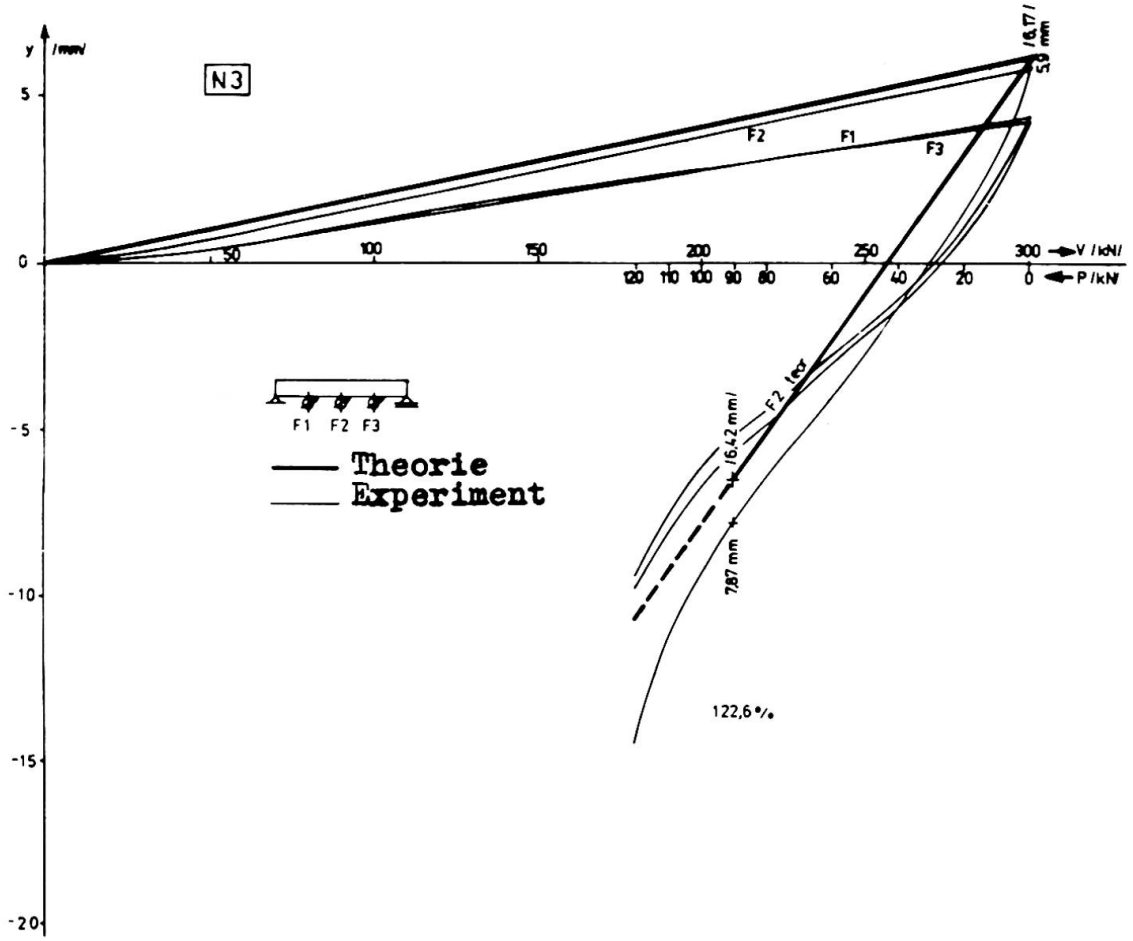

Bild 9. Durchbiegungen y des Trägers N 3 in Abhängigkeit von der Vorspannung V und Belastung P

In den Diagrammen, von denen eines am Bild 9 gezeigt wird, sind numerisch Kontrollwerte bei der Vorspannkraft V = 300 kN angegeben. Die theoretische Durchbiegung ist 6,17 mm /100%/; der durchschnittliche Wert aus den gemessenen Durchbiegungen ist 5,71 mm /92,5%/, also nur wenig geringer als berechnet. In den meisten Fällen wuchs die Durchbiegung linear.

- Wenn ausser der Vorspannung noch eine vertikale Belastung wirkte, waren die maximalen Durchbiegungen im Durchschnitt um 37% grösser als berechnet. Die Durchbiegungen waren grundsätzlich in guter Übereinstimmung mit den Spannungen, die gleichfalls höher waren als die berechneten.

Die Verschiedenheit der konstruktiven Lösung hat sich auf die Trägertragfähigkeit nicht ausgewirkt: Der Walzträger I PE hat einen genügend dicken Steg, so dass er hohe Einzellasten überträgt ohne dass der nicht ausgesteifte Steg lokal ausbeulte /I PE 30 überträgt verlässlich die Lasten 3x126 kN/. Der starke Untergurt braucht keine dichte Anordung der stabilisierenden Diafragmen. Auch ein Träger ohne stabilisierende Diafragmen übertrug eine Vorspannkraft von 400 kN /also um 100 kN mehr als der verlangte Wert/.

Die Prüfungen haben bestätigt, dass durch Vorspannung mittels eines hochfesten Zugbandes die Tragfähigkeit der Walzträger bedeutend erhöht werden kann, besonders im elastischen Bereich. Die Tragfähigkeit wächst weiter, wenn die plastische Reserve des Stahles

genützt wird. Die Ausnutzung der plastischen Reserve stösst auf Probleme der Stabilität. Infolge der Vorspannung, Nutzung der plastischen Reserve des Materials und bedeutend hoher Fliessgrenze des verwendeten Stahls erreichte man in 2/3 der Fälle der angeführten Experimente eine doppelte Tragfähigkeit gegenüber der, die die Berechnung des nicht vorgespannten Trägers /2/ ergibt.

Literatur:

/1/ Ferjenčík, P. - Tocháček, M.: Skúšky predpätých oceľových nosníkov v pružnom a pružnoplastickom stave. Druhá dielčia etapa úlohy P 12-124-003-02/2,e Predpäté kovové a lanové konštrukcie. Bratislava, KKDK SvF SVŠT, 1975.

/2/ ČSN 73 1401 Navrhování ocelových konstrukcí. Praha ÚNM /Gültigkeit ab 1. 1. 1968/.

Behaviour of Hybrid Beam-Columns under Cyclic Loading

Comportement de montants hybrides soumis à des flexions cycliques

Verhalten von hybriden Stahlstützen unter zyklischer Biegebeanspruchung

M. YAMADA Prof.
B. TSUJI Prof.
Faculty of Engineering, Kobe University
Kobe, Japan

1. INTRODUCTION

The cyclic bending deformation behavior of the wide flange section was discussed by the senior auther(1),(2), and it was clarified that the cyclic bending moment-curvature relationship under the constant axial force asymptotes to the relationship of the pure bending due to the strain hardening effect. The cyclic bending behavior of the hybrid member is discussed here.

2.ANALYSIS

2.1. Analytical Model

A wide flange section is simplified into a three points model(2) such as shown in Fig.1. The area of the web is k times the one of the flange. The yield stress σ_{yw} of the web is ρ times the yield stress σ_{yf} of the flange. The stress-strain relationship of the material is tri-linear type such as shown in Fig.2. In general, with the increase of the yield stress σ_y, the yield ratio $\zeta=\sigma_y/\sigma_{max}$ increases and the strain hardening coefficient $\mu=E_{st}/E$ decreases. Fig.3 shows the relationship between the yield ratio ζ or the strain hardening coefficient μ and the yield stress σ_y. Indicating the stresses of each point as $\bar{\sigma}_i=\sigma_i/\sigma_{iy}(i=1,2,3)$, the axial force $N=nN_y$ and the bending moment $M=mM_y$ are obtained as follows:

$$n=\frac{\bar{\sigma}_1+\bar{\sigma}_3+\rho k\bar{\sigma}_2}{2+\rho k}$$

$$m=\frac{\bar{\sigma}_1-\bar{\sigma}_3}{2}$$

The stresses of each point are obtained by summation of the elastic stress and the residual stress such as shown in Fig.4, and are represented as follows:

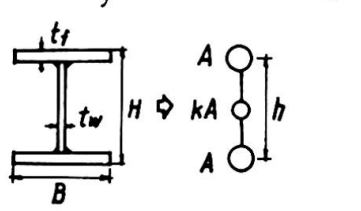

Fig.1 Three Points Model

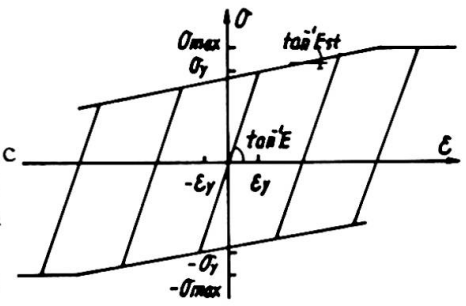

Fig.2 σ - ε Relationship

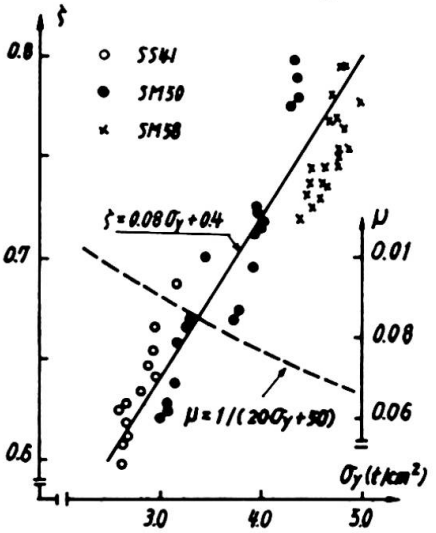

Fig.3 Yield Ratio ζ and Strain Hard. Coeff. μ

$$\bar{\sigma}_1=(2+\rho k)/(2+k)n+m+\xi$$

$$\bar{\sigma}_2=(2+\rho k)/\rho(2+k)n-2\xi/\rho k$$

$$\bar{\sigma}_3=(2+\rho k)/(2+k)n-m+\xi$$

where ξ is a parameter indicating the magnitude of the residual stress. The yield conditions of each point are as follows:

$$\alpha_i-2\leq\bar{\sigma}_i\leq\alpha_i$$

$$-1/\zeta_i\leq\bar{\sigma}_i\leq 1/\zeta_i$$

where α_i shows the subsequent yield stress. Fig.5 shows the yield polygon. The broken line shows the envelope of the yield polygon and a stress point can not go out of this range.

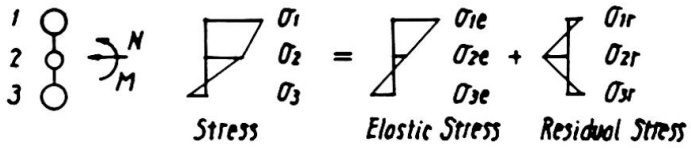

Fig.4 Stress Distribution

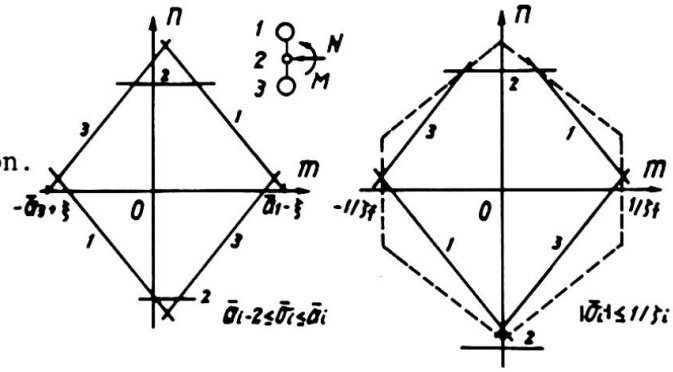

Fig.5 Yield Conditions

2.2. Bending Moment-Curvature Relationship

Fig.6 shows the bending moment-curvature relationship under the constant axial force of $N=0.5N_y$. Four types of the cross section computed are shown in Table 1. Figs.(a) and (b) correspond to the homogeneous members using a mild steel and a high strength steel, and Figs.(c) and (d) to the hybrid member using a high strength steel as the flange and the web, respectively. In each case, the relationships converge to the steady state loop at the three or four cycles. In the case of type A and D, the relationships converge to those of the pure bending due to the strain hardening effect, whereas in the case of type B and C, the loops converge to the steady state ones, the maximum bending capacity of which is somewhat smaller than that of the former case, due to the fully plastic state of the web and the compression flange.

Table 1 Types of Members

	Type	σ_{yf}(t/cm^2)	σ_{yw}(t/cm^2)
Homogeneous Member	A	3.0	3.0
	B	5.0	5.0
Hybrid Member	C	5.0	3.0
	D	3.0	5.0

σ_y(t/cm^2)	$\mu=E_{st}/E$	$\zeta=\sigma_y/\sigma_{max}$
3.0	1/110	0.64
5.0	1/150	0.80

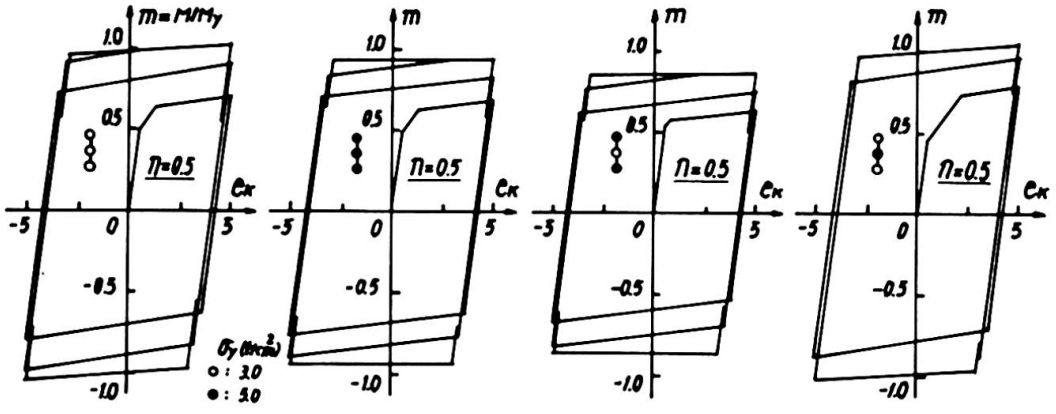

(a) Type A (b) Type B (c) Type C (d) Type D

Fig.6 Bending Moment-Curvature Relationship

2.3. Load-Deformation Relationship

Fig.7 shows the lateral load-deflection relationship of the column, the slendreness ratio of which is 25, under the constant axial load of $N=0.5N_y$. Alternately repeated horizontal force $P=pP_y$ is applied at the constant lateral

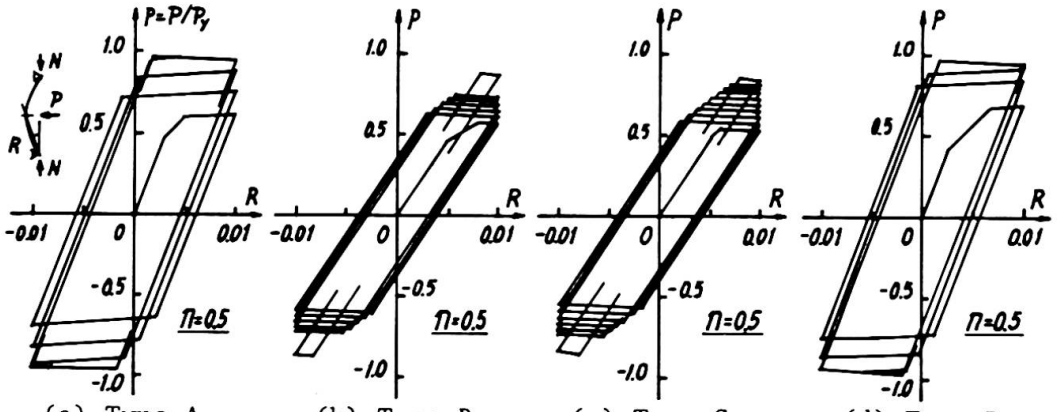

(a) Type A (b) Type B (c) Type C (d) Type D

Fig.7 Load-Deformation Relationship

sway rotation angle of R=±0.01. Figs.(a) and (b) correspond to the homogeneous member and Figs.(c) and (d) correspond to the hybrid one. In the case of the columns having a mild steel flange (type A and D), the load-deflection relationships converge to the steady state loop at the few cycles because of the small yield ratio (ζ=0.64) and of the large strain hardening coefficient (μ=1/110). The relationships of type B and C columns having high strength steel flange converge to the steady state loop at 17 and 13 cycles,respectively.

2.4. Variation of Maximum Strength and Accumulated Plastic Strain

Fig.8 shows the relationship between the maximum strength and the number of cycles. The abscissa W shows the number of half cycles. The maximum strength increases with the number of cycles. The strength of the hybrid member using a high strength steel as the web (type D) is the largest and using a mild steel as the web is the smallest. Convergence to the steady state loop is rapid in the case of the member having mild steel flange. Fig.9 shows the variation of the accumulated plastic strain of the web. The accumulated plastic strain induced is large in the case of a hybrid member using the mild steel web, and small in the case of the member using high strength steel web. In some cases, the plastic strain increases with the number of cycles even after the maximum strength converges to the steady state value.

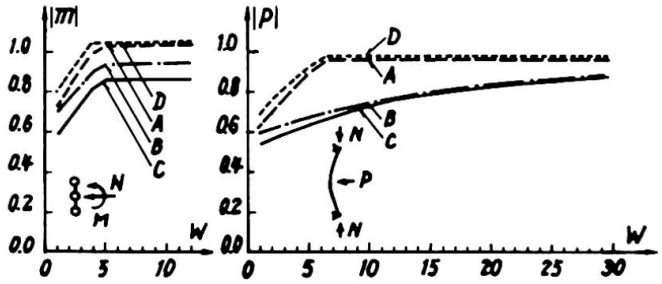

Fig.8 Variation of Maximum Strength

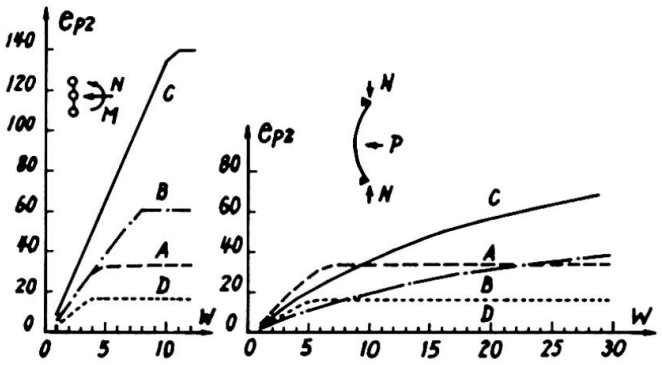

Fig.9 Accumulated Plastic Strain

3.CONCLUDING REMARKES

Elastic plastic behavior of the wide flange columns with homogeneous and hybrid sections was discussed. In the case of the members having high strength steel with large yield ratio and small strain hardening coefficient, the increase in the strength under the cyclic loading is relatively small. The hybrid member having a mild steel web shows a relatively small increment in the strength under the cyclic loading and induces the large amount of accumulated plastic strain in the web even under the small axial force range.

On the other hand, the hybrid member having a high strength steel web shows a relatively large increment in the strength and induces relatively small amount of plastic strain in the web.

BIBLIOGRAPHY

(1) Yamada,M. : Freie Diskussion IIIc, Final Report, 8th. Congr., IABSE, New York, 1968, pp.693-695.
(2) Yamada,M., Shirakawa,K. : Elaso-plastische Biegeformänderungen von Stahlstützen mit I-Querschnitt, Teil II : Wechselseitig wiederholte Biegung unter konstanter Normalkrafteinwirkung, Der Stahlbau, 40. Jahrg., H.3, 1971, S. 65-74 u. H.5, 1971, S.143-151.
(3) Horikawa,K. : Experimental Study on Shape and Size of Tensile Specimen, JSSC, Vol.5, No.48, 1969, pp.52-67, (in Japanese).

SUMMARY

Elasto-plastic cyclic bending deformation behaviour of the hybrid members is discussed assuming a wide flange section as a three points model and stress-strain relationship as tri-linear type. In the case of the hybrid member, the increase in the strength under the cyclic loading are larger and the amount of the accumulated plastic strains are smaller for the member with weaker flange than with weaker web. The limiting axial force level within which the bending resistance of the column asymptotes to that of pure bending is lower for the weaker web member.

RESUME

Les auteurs présentent le comportement élasto-plastique d'éléments hybrides soumis à des flexions cycliques; ils remplacent le profilé à larges ailes étudié par un modèle à trois surfaces et admettent une relation contraintes-allongements du type trilinéaire. Pour des éléments hybrides possédant un âme en acier à haute résistance, l'augmentation de résistance sous charges cycliques est plus élevée et la quantité de déformations plastiques accumulées, plus faible que pour une âme en acier doux. L'effort normal limite permettant asymptotiquement un moment de ruine égal à celui correspondant à la flexion pure est moins élevé lorsque l'âme est en acier doux.

ZUSAMMENFASSUNG

Das elasto-plastische Biegeverformungsverhalten einer zyklisch beanspruchten hybriden Stahlstütze ist unter der Annahme eines drei Punkt-Modelles des Breitflansc Querschnittes und einer tri-linearen Vereinfachung der σ-ε-Beziehung untersucht. Im Fall von hybriden Stahlstützen mit schwächerem Flansch ist der Zuwachs des Widerstandes grösser und die Verzerrungsakkumulation kleiner als für Querschnitte mit schwächerem Steg. Der Grenzwert des Normalkraftniveaus,für das der Biegewiderstand mit demjenigen unter reiner Biegung asymptotisch übereinstimmt, ist niedriger für einen Querschnitt mit schwächerem Steg.

On Structural Behaviour of Hybrid I-Beams

Sur le comportement à la ruine des poutres en I hybrides

Zum Tragverhalten hybrider I-Balken

ZBIGNIEW CYWIŃSKI
Assistant Professor
Technical University of Gdańsk
Gdańsk, Poland

This contribution refers to Theme Va of the Introductory and Preliminary Reports. It represents certain proposal for the plastic analysis of hybrid I-beams assuming combined action of bending and shear.

Author's treatment of mentioned problem bases upon that suggested by Strel'bitskaya for homogeneous beams /1/. Simultaneously Schilling's optimum design criteria are taken into account /2/. Collapse loads determined are compared with those resulting from the ASCE-AASHO regulations /3/.

Plastic bending-shear interaction analysis of homogeneous I-beams bases generally on the yield condition

$$\sigma^2 + 3\tau^2 = \sigma_0^2 , \qquad (1)$$

where σ , τ are the elastic bending and shear stresses, respectively, and σ_0 is the yield stress. According to /1/ the elastic stress patterns are as shown in Fig. 1; both of them are more (σ) or less (τ) inaccurate but fulfil the yield condition (1) at each point of the I-section and develop sufficiently exact (conservative) collapse load values. Similar analysis of hybrid I-beams can be based on stress patterns as given in Fig. 2.

With the specifications of Fig. 2 the fully plastic moment and shear, M_0 and Q_0 respectively, can be expressed as follows:

$$M_0 = \sigma_0 \frac{A_f h}{2} + \alpha \sigma_0 \frac{th^2}{4} = \sigma_0 \frac{th^2}{4}(1+\alpha), \qquad (2)$$

$$Q_0 = \alpha \tau_0 th = \sigma_0 \frac{th}{\sqrt{3}} \alpha , \qquad (3)$$

whereby the following numerical values of α and σ_0 are being considered:

$\alpha = 1.00$, for $\sigma_0 = 36{,}000$ psi (homogeneous beam),
$\alpha = 0.72$, for $\sigma_0 = 50{,}000$ psi
$\alpha = 0.36$, for $\sigma_0 = 100{,}000$ psi (hybrid beams).

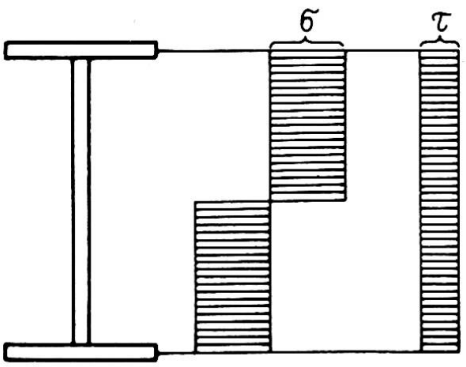

Fig. 1. Elastic stress patterns for homogeneous I-beam; assumed in [1]

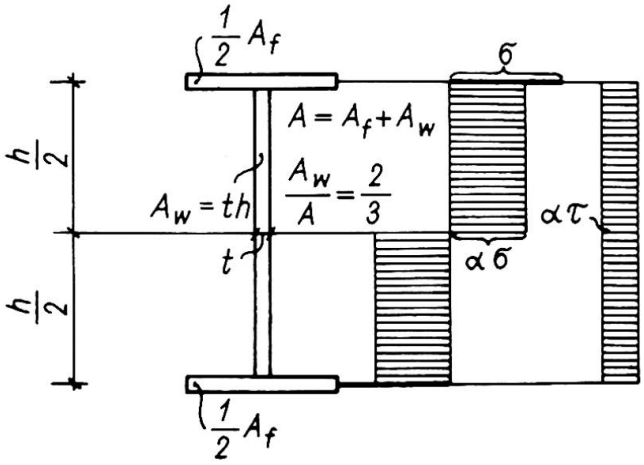

Fig. 2. Elastic stress patterns for hybrid I-beam; Author's assumption

Investigations performed concern in particular the beam fixed at both ends carrying single load P at span-mid or uniform load q all over the span (Fig. 3).

According to Author

$$P = \frac{8\,\frac{M_o}{l}}{\sqrt{\frac{16\,M_o^2}{l^2\,Q_o^2}+1}} = \frac{8\,\frac{M_{ou}}{l}}{\sqrt{12\left(\frac{h}{l}\right)^2+\left(\frac{2\alpha}{1+\alpha}\right)^2}}$$

$$q = \frac{16\,\frac{M_o}{l^2}}{\frac{16\,M_o^2}{l^2\,Q_o^2}+1} = \frac{16\,\frac{M_{ou}}{l^2}}{6\left(\frac{h}{l}\right)^2\frac{1+\alpha}{\alpha}+\frac{2\alpha}{1+\alpha}}$$

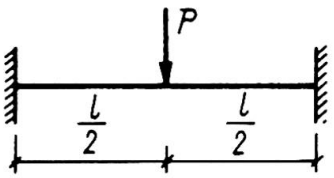

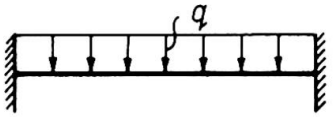

According to ASCE-AASHO

$$P = \frac{16\,\frac{M_o}{l}}{\sqrt{64\,\frac{M_o^2}{l^2\,Q_o^2}\,\frac{\alpha}{1+\alpha}+1}+1} = \frac{8\,\frac{1+\alpha}{\alpha}\,\frac{M_{ou}}{l}}{\sqrt{12\left(\frac{h}{l}\right)^2\frac{1+\alpha}{\alpha}+1}+1}$$

$$q = \frac{32\,\frac{M_o}{l^2}}{\sqrt{128\,\frac{M_o^2}{l^2\,Q_o^2}\,\frac{\alpha}{1+\alpha}+1}+1} = \frac{16\,\frac{1+\alpha}{\alpha}\,\frac{M_{ou}}{l^2}}{\sqrt{24\left(\frac{h}{l}\right)^2\frac{1+\alpha}{\alpha}+1}+1}$$

Fig. 3. General expressions of collapse loads

Extending the interaction formula of /1/

$$\frac{M^2}{M_o^2} + \frac{Q^2}{Q_o^2} = 1 \tag{4}$$

over to hybrid I-beams and taking into account the corresponding equation

$$\frac{M}{M_o} + \frac{Q^2}{Q_o^2}\,\frac{\alpha}{1+\alpha} = 1$$

resulting from ASCE-AASHO regulations /3/ a set of general collapse load expressions can be obtained which is given in Fig. 3; therein

$$M_o = \frac{1+\alpha}{2\alpha}\,M_{ou} \tag{5}$$

where $M_{ou} \equiv M_o(\alpha=1)$ holds for homogeneous (uniform) beam.

On the basis of the expressions derived the corresponding interaction curves, in terms of Pl/M_{ou} and ql^2/M_{ou} respectively, as functions of the span-depth ratio l/h can be found; this is illustrated in Fig. 4 and Fig. 5.

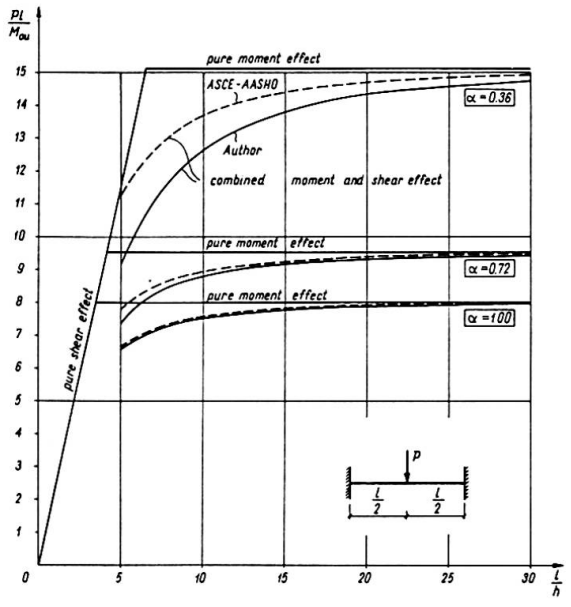

Fig 4 Collapse loads - concentrated

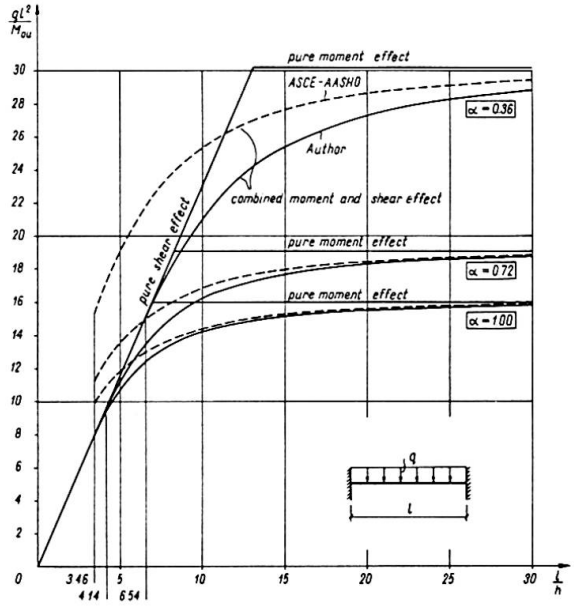

Fig 5 Collapse loads - uniform

In conclusion Author's proposal can be characterized as follows:

1. It yields collapse loads close (conservative) to those of the ASCE-AASHO regulations whereby the relative difference increases with a decrease of the l/h-ratio and the α-value.
2. It visualizes clearly the dominating effect of pure shear for small l/h-ratios.
3. It can be found handy analysing non-uniform plastic torsion problems (bimoment - flexural-torsional moment interaction, St.-Venant torsional moment effect) of hybrid sections, as shown for the homogeneous ones in /1/ and /4/.

References

/1/ Strel'bitskaya, A.I.: A study of strength of thin-walled beams beyond the elastic limit (in Russian). Izdatel'stvo AN USSR, Kiev 1958.

/2/ Schilling, Ch.G.: Optimum properties for I-shaped beams. Journal of the structural Division, ASCE, Vol. 100, No. ST 12, Dec. 1974, pp. 2385-2401.

/3/ Design of hybrid steel beams. Report of the Subcommittee 1 on Hybrid Beams and Girders of the Joint ASCE-AASHO Committee on Flexural Members. Journal of the Structural Division, ASCE, Vol. 94, No. ST 6, June 1968, pp. 1397-1426.

/4/ Strel'bitskaya, A.I.: Limit state of frames out of thin-walled members in bending with torsion (in Russian). Izdatel'stvo AN USSR, Kiev 1964.

SUMMARY

Simplified procedure is used to determine the ultimate load of hybrid I-beams in combined bending with shear. It has been found sufficiently exact and is recommended for analysis of similar problems within the theory of non-uniform torsion.

RESUME

Pour la détermination de la charge ultime de poutres hybrides en I soumises à la flexion et au cisaillement, on applique une méthode simplifiée. Celle-ci a donné des résultats suffisamment précis et est recommandée pour la résolution des problèmes similaires dans la théorie de torsion non uniforme.

ZUSAMMENFASSUNG

Ein vereinfachtes Verfahren wurde benutzt, um die Traglast hybrider I-Balken bei zusammengesetzter Biegung mit Schub zu bestimmen. Dieses wurde ausreichend genau gefunden und wird zur Behandlung benachbarter Probleme innerhalb der Theorie der Wölbkrafttorsion empfohlen.

Comportement à la fatigue des poutres hybrides raidies

Ermüdungsverhalten von ausgesteiften hybriden Trägern

Fatigue Behaviour of Stiffened Hybrid Beams

ANDRÉ PLUMIER
Ingénieur aux Laboratoires d'Essais des Constructions du Génie Civil
Université de Liège
Liège, Belgique

Cette étude, financée par la CECA et le CRIF et réalisée sous la direction du Professeur R. BAUS, concerne des poutres hybrides dont les semelles sont en acier E 70 et dont l'âme et les raidisseurs sont en acier E 27 ; quelques poutres homogènes en acier E 70 ont également été testées. Les poutres comportent des raidisseurs soudés aux deux semelles, à l'exception d'une poutre hybride et d'une poutre homogène dont les raidisseurs ne sont soudés qu'à la semelle comprimée ; par ailleurs, une des poutres hybrides comporte une série de goussets soudés à la semelle tendue. Les dimensions générales des poutres et la mise en charge sont schématisées à la figure 1.

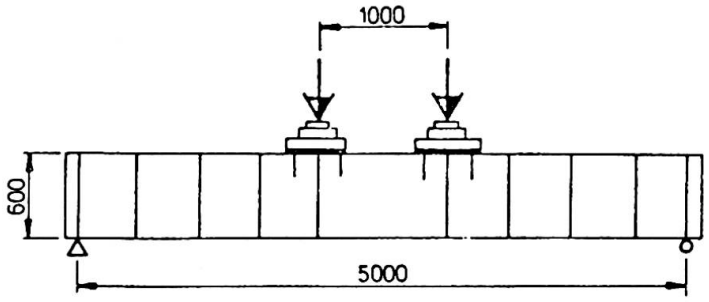

Schéma du montage d'essai

Figure 1

On diffuse les charges appliquées au moyen de plats de forte épaisseur, de plaques de néoprène et de goussets complémentaires. Les types de fissures observés sont présentés à la figure 2.

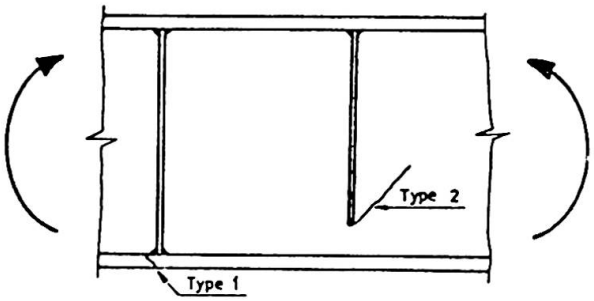

Types de fissure

Figure 2

Les résultats des essais sont donnés à la figure 3, pour les fissures du type 1.

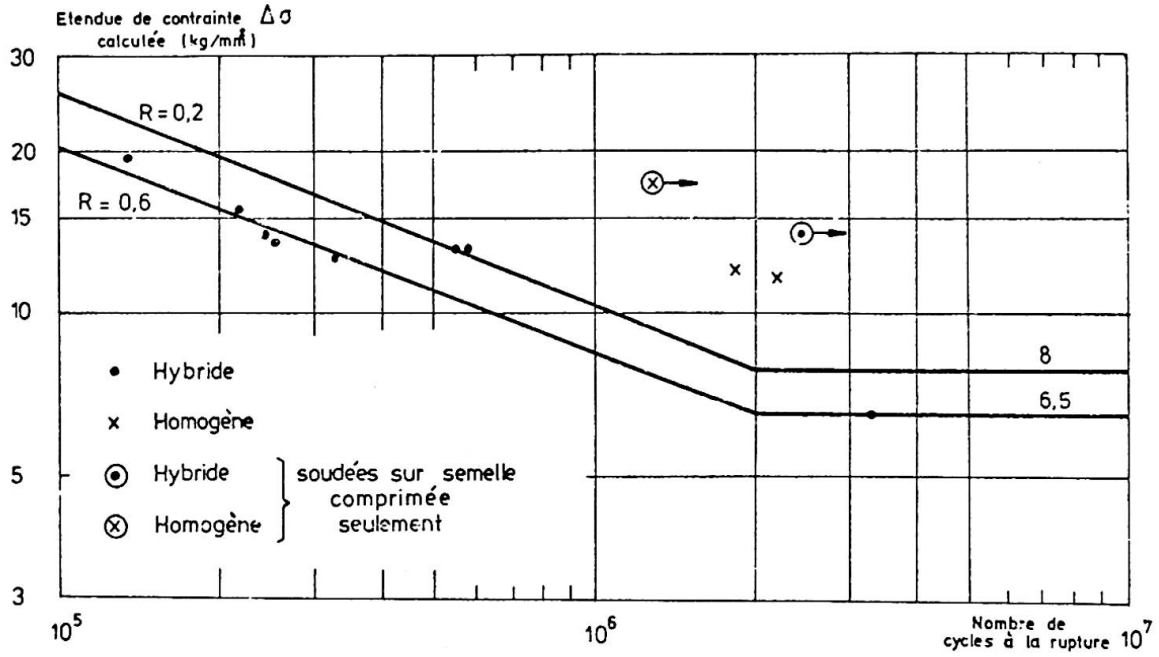

Courbes ΔO - N pour les fissures du type 1

Figure 3

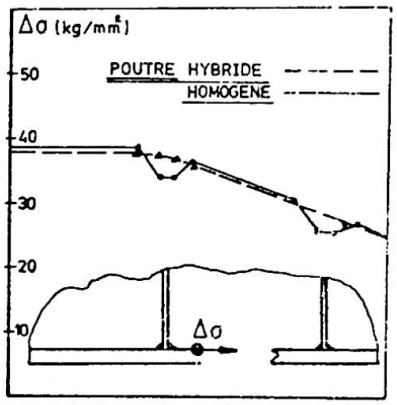

Distribution des ΔO de service

Figure 4

On donne à la figure 4 la distribution des étendues de contraintes Δσ mesurées en service à la fibre intérieure de la semelle tendue entre les charges maximales et minimales. On constate une différence marquée entre la poutre hybride, dans laquelle la plastification initiale égalise les étendues de contrainte en service et la poutre homogène, dans laquelle le raidisseur reste un point dur engendrant une flexion locale.

Des essais effectués, on peut tirer les conclusions suivantes :

1° La résistance en fatigue correspondant à l'assemblage du raidisseur à la semelle est, dans le cas des poutres hybrides, voisine de celle des poutres homogènes classiques ;

2° Dans les poutres hybrides cette résistance ne paraît pas différente selon que le raidisseur est fixé aux deux semelles ou seulement à la semelle tendue, ou selon qu'il se trouve, ou non, sous la charge ; ceci peut être expliqué par l'égalisation des contraintes mentionnée plus haut ;

3° Dans les poutres hybrides, l'étendue des contraintes mesurées en service au niveau du cordon d'assemblage des raidisseurs est égale à la valeur calculée ; dans les poutres homogènes, elle est de 10 % inférieure à la valeur calculée. Ce fait et le meilleur profil des cordons réalisés sur les poutres homogènes expliquent leurs résultats légèrement supérieurs ;

4° De cette constatation, on peut conclure que les résultats des essais sur modèles de grande dimension doivent être étudiés avec circonspection, car les effets locaux du comportement structurel entraînent une différence entre les contraintes réelles et calculées au droit du cordon de soudure.

5° L'hypothèse selon laquelle, par suite de l'existence de contraintes résiduelles, il faut considérer que tout joint soudé d'une pièce soumise à fatigue travaille en traction entre unecontrainte maximale égale à la limite élastique de l'acier et une contrainte inférieure à celle-ci [1] constitue une simplification sécuritaire. Ni dans les essais effectués à Liège, ni en [2], il n'a été observé de fissuration au départ d'un joint de raidisseur à une semelle comprimée, même pour de grandes étendues de contraintes et en dépit de l'existence de contraintes résiduelles de traction particulièrement élevées (70 kg/mm2). On peut penser que la fissuration n'apparaît en zone comprimée qu'en présence d'actions locales de cisaillement ou de flexion [2], souvent ignorées lors du calcul des éléments.

6° Il convient d'éviter la soudure de raidisseurs sur la semelle tendue dans les zones de grands moments de flexion.

BIBLIOGRAPHIE.

[1] T.R. GURNEY et S.J. MADDOX. A re-analysis of fatigue data for welded joints in steel. W.I. Report E/44/72.

[2] Y. MAEDA, MI. ISHIWATA,Y. KAWAI. Structural Behaviour of Hybrid Plate Girders in Bending - Preliminary Report of the 10th Congress of IABSE.

RESUME

La résistance des poutres hybrides raidies aux sollicitations dynamiques est un peu inférieure à celle des poutres homogènes, en raison de certaines particularités du comportement structurel.

ZUSAMMENFASSUNG

Das Ermüdungsverhalten von ausgesteiften hybriden Trägern ist leicht weniger günstig als dasjenige von homogenen Trägern, wegen der besonderen örtlichen Spannungsverteilung in der Umgebung der Steifen.

SUMMARY

The resistance of stiffened hybrid beams to dynamic loads is a little less than that of homogenous beams, because of a particular stress distribution near the stiffener.

Leere Seite
Blank page
Page vide

Additional Tests for "Type 2 Crack" in Hybrid Girders

Essais complémentaires pour les fissures de "type 2" dans les poutres hybrides

Zusätzliche Versuche bezüglich der Risse von "Typ 2" in hybriden Trägern

Y. MAEDA
Professor of Civil Engineering
Osaka University
Suita, Osaka, Japan

M. ISHIWATA
Senior Engineer
Kawasaki Steel Co., Ltd.
Tokyo, Japan

Y. KAWAI
Research Engineer
Kawasaki Steel Co., Ltd
Chiba, Japan

1. Introduction

At the Preliminary Report of the 10th Congress of IABSE[1)], we pointed out that the fatigue failure of thin-walled hybrid girders is generally due to "Type 2 Cracks" initiated at transverse stiffener-to-web fillet weldments. Further, a good correlation between the large-sized girder test results and the small-sized model test results using a steel plate with a transverse fillet welded attachment, was demonstrated. The girder tests, however, were not sufficient in numbers to warrant the fatigue strength, and the model tests did not exactly simulate the structural behavior of the girders because of the difference of strain states.

We are now presenting the results of additional fatigue tests, which have been carried out on axially loaded transverse non-load-carrying fillet welded specimens under strain control to examine the fatigue strength of "Type 2 Cracks" in hybrid girders.

2. Tests

Transverse non-load-carrying fillet welded specimens, as shown in Fig. 1, intended for simulating the boxing parts of the transverse stiffener-to-web fillet welds in hybrid girders, are axially loaded under strain control by fixing the out-put of strain gauges on the specimens to the maximum strain of 1700×10^{-6}, which corresponds to the design working strain of 80 kg/mm^2 high strength steel in a tension flange of girders.

The specimens consist of JIS-SS41 steel with a specified tensile strength of 41 kg/mm^2, and are divided into two series, namely, the ones of which at weld toe are as-welded and the others are lightly ground at the toe to examine the effect of finishing. Such a test simulates the structural behavior proper

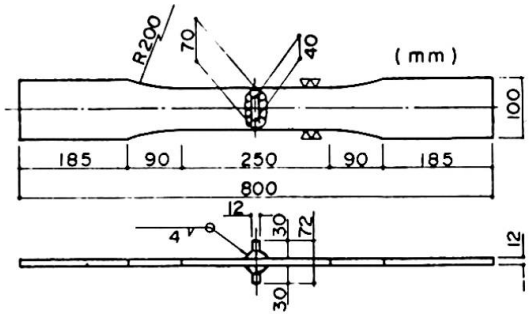

Fig.1 Details of As-Welded Specimen

to hybrid girders that a web reaches a kind of strain-controlled state after yielding due to the contribution of elastic frame action of flanges to the restraining of plastic flow of the web.

3. Results

The test results are graphically shown on the S-N diagram in Fig.2, in terms of equivalent stress range due to the strain range versus number of cycles to failure, neglecting the effect of stress ratios. The fatigue strength at 2×10^6 cycles of the as-welded specimens and of the lightly-ground specimens can be estimated at 9.5 kg/mm^2 and 10.5 kg/mm^2 as the mean value of stress ranges, respectively. The effect of finishing on the fatigue strength is not so remarkable at the present tests. This may be attributed to the fact that the grind operation was not fully performed and consequently some fine notches were not removed.

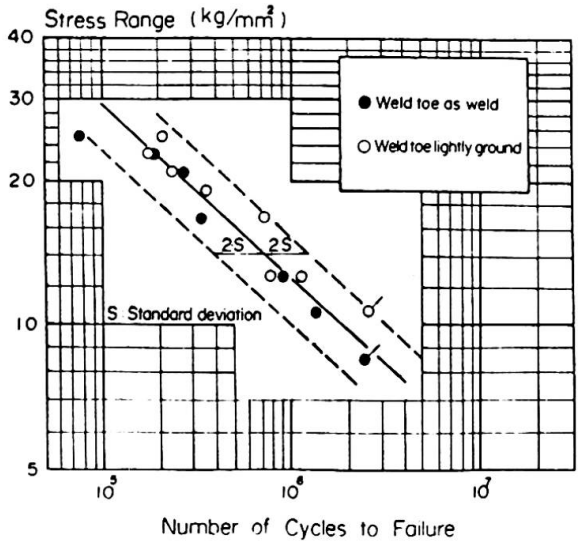

Fig.2 Fatigue Test Results

4. Discussions

(1) To study the influence of load controlling method on fatigue lives, comparison of the present test results with previous fatigue data on model specimens with the same configuration as the present ones, which were given by reanalysis of Gurney et al[2] about numerous tests, is shown in Fig.3.

It can be seen that the present test results, unexpectedly, agree well with the reanalyzed S-N curve by Gurney et al, which took into account the effect of residual stress on fatigue. It may be recognized that such a good agreement was obtained, because the correction of S-N curves was done on the assumption that residual stresses resulting from welding would generally be as high as the yield stress of the parent material as expected in a large as-welded structure, and such an assumption can be applied to the present tests,

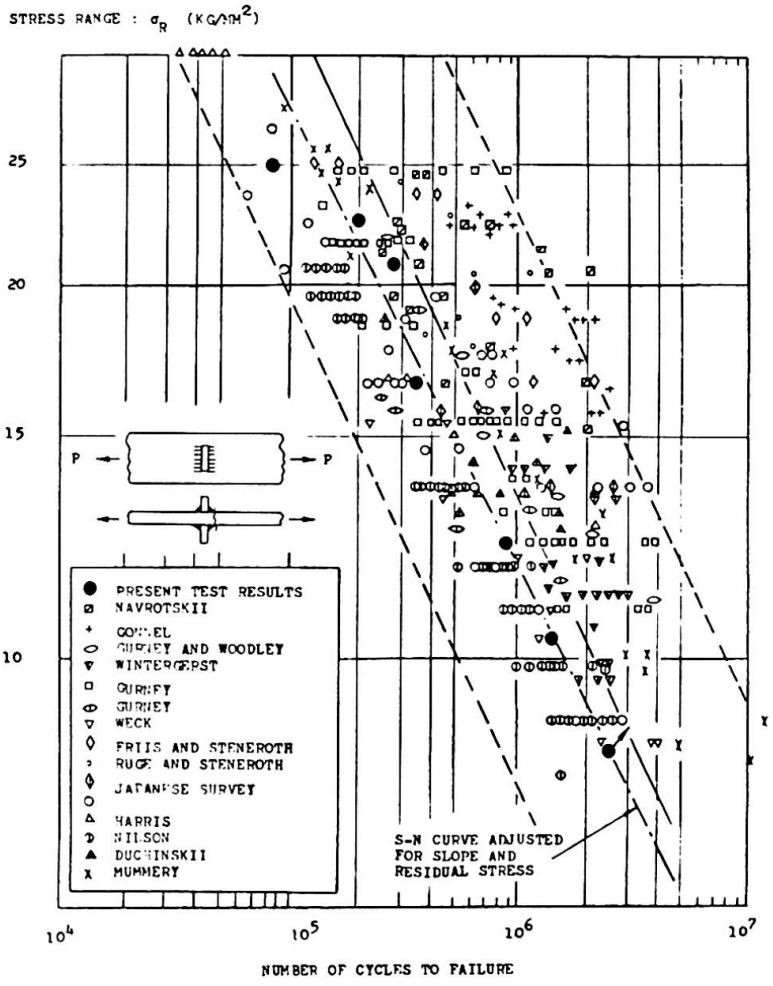

Fig.3 S-N Curves for Transverse Non-Load-Carrying Fillet Welded Joints

in which the specimens could yield at the maximum loading controlled by the strains.

(2) To study on the effect of steel grades on the fatigue strength, another comparison of the present test results for as-welded specimens with other steels[3], is made as shown in Fig. 4. Here, JIS-SM58 and WES-HT80 are high-strength steels with a specified tensile strength of 58 kg/mm^{2}and 80 kg/mm^2, respectively. The latter specimens are provided with the same configuration as the present test specimens, but their loading was controlled by loads from zero to tension.

Since any significant difference among those data cannot be observed, it will be concluded that, at such a welded joint with a large notch effect, the fatigue strength in terms of stress ranges are almost identical one another regardless of steel grades, stress ratios and load-controlling methods.

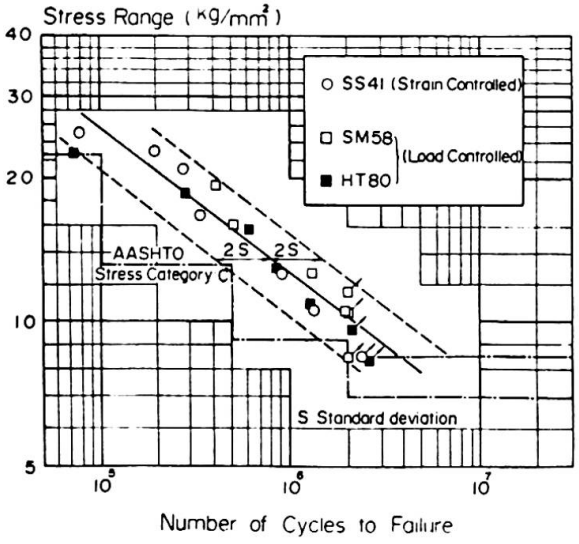

Fig.4 Fatigue Strength of Transverse Non-Load-Carrying Fillet Welded Joints for SS41, SM58 and HT80

(3) Finally, the relation between girder fatigue tests[1),4)] and some model fatigue tests is shown in Fig.5 . The model test results consist of the present test results and the previous ones in Japan [5),6)] on steel plates with transverse fillet welded attachments without boxing. The figure reveals that the present test results under relatively severe loading conditions, can be compared well with the lower 95 % confidence limit line of all the quoted test results except the present test results, and this implies that the present test results give conservative fatigue strengths due to "Type 2 Cracks" in hybrid girders.

It can be also noticed that the allowable fatigue stresses for "Stress Category C" specified at AASHTO Interim Specifications[7)], 1974, are reasonable for "Type 2 Cracks" in hybrid girders as seen in Fig. 4.

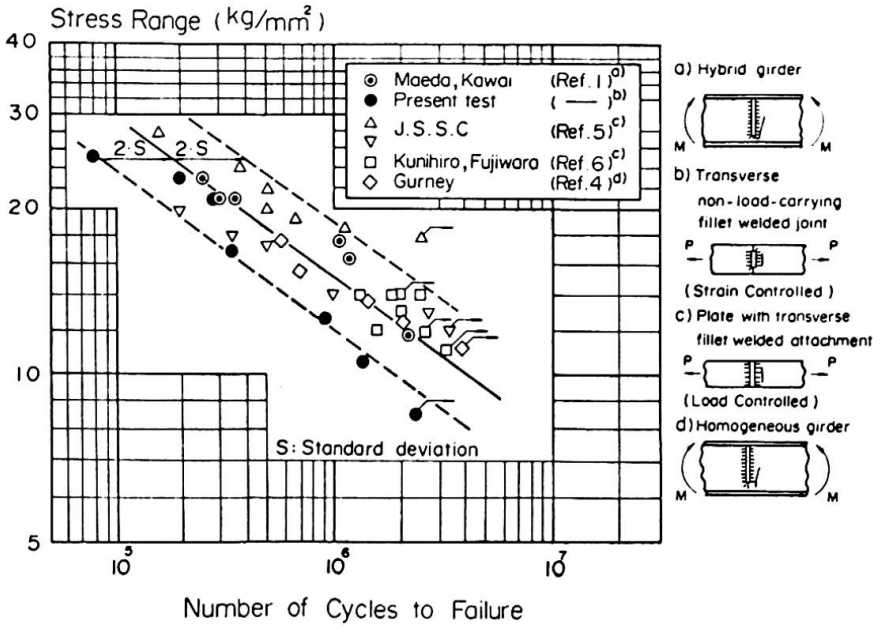

Fig.5 Comparison of Fatigue Strength for Type 2 Cracks in Girder Tests with Model Specimen Tests

References:

1) Y. Maeda, M. Ishiwata and Y. Kawai, Preliminary Report of the 10th Congress of IABSE, 1976.
2) T.R. Gurney and S.J. Maddox, The Welding Institute Research Report, E/44/72, 1972.
3) M. Ishiwata, Y. Tanaba, H. Yukitomo and Y. Kawashima, Preprints of the 26th National Conf. of the Japan Society of Civil Engineers, 1971 (in Japanese).
4) T.R. Gurney and C.C. Woodley, British Welding J., Vol.9, Sept., 1962.
5) J. of the Jpan Society of Steel Construction, Vol.7, No.72, 1971 (in Japanese).
6) T. Kunihiro and M. Fujiwara, Tech. Rept. on Civil Engineering, Vol.14, No.2, Tokyo, 1972 (in Japanese).
7) AASHTO, Interim Specification for Bridges - Interim 8, 1974.

SUMMARY

To supplement the paper presented by the same authors at the Preliminary Report on "Structural Behaviour of Hybrid Girders in Bending and Application to Actual Bridges", additional tests on "Type 2 Cracks" are reported with the results and the discussions. It will be concluded that the fatigue strengths for Type 2 cracking are almost identical one another regardless of steel grades, stress ratios and load-control methods.

RESUME

Pour compléter la contribution présentée par les mêmes auteurs dans le Rapport Préliminaire, "Comportement à la flexion de poutres à âme pleine hybrides. Application aux ponts actuels", des essais complémentaires ont été réalisés pour étudier les fissures de"type 2". Résultats et discussions sont présentés. Il est possible de conclure que les résistances à la fatigue correspondant aux fissures de "type 2" sont pratiquement les mêmes, et indépendantes du type d'acier et de la contrainte moyenne.

ZUSAMMENFASSUNG

Um den von den gleichen Autoren im Vorbericht erschienenen Beitrag zu ergänzen ("Biegeverhalten von hybriden Vollwandträgern. Anwendung im Brückenbau"), wurden zusätzliche Versuche zur Untersuchung von "Typ 2" Rissen durchgeführt. Ergebnisse und Diskussion werden dargestellt. Die Schlussfolgerung lautet, dass die den Rissen "Typ 2" entsprechenden Ermüdungsfestigkeiten praktisch gleich sind, unabhängig von der Stahlfestigkeit und von der mittleren Spannung.

Fatigue Life Prediction of Hybrid Members

Prédiction de la résistance à la fatigue d'éléments hybrides

Vorhersage der Lebensdauer von auf Ermüdung beanspruchten hybriden Elementen

T. YAMASAKI, General Manager
M. HARA, Senior Research Engineer
Y. KAWAI, Research Engineer
Structure Research Center, Kawasaki Steel Co., Ltd.
Chiba, Japan

1. INTRODUCTION

In the Preliminary Report for 10th Congress of the IABSE, 1976, fatigue crack growth rate observations were illustrated on the hybrid tee-shaped specimens to explore a possibility of the estimation of fatigue lives by using fracture mechanics(1).

Additional fatigue crack propagation test was conducted on a center-notched hybrid plate specimen to warrant the fatigue life prediction method for hybrid members.

2. FATIGUE CRACK PROPAGATION TEST

The configuration of the specimen is shown in Fig.1. One specimen consisting of JIS-SS41 (with specified tensile strength of 41 kg/mm^2) and WES-HW70 (with specified tensile strength of 80 kg/mm^2) was longitudinally butt welded along the specimen center line, and an artificial notch was introduced into its center to start a fatigue crack. The chemical analysis and mechanical properties of the materials are shown in Table 1.

The fatigue test was carried out in a 100-ton electro-hydraulic alternating testing machine under stress ranges of 15 kg/mm^2 and 10 kg/mm^2 and at a stress ratio of zero. Fatigue crack growth rate was observed on both the SS41 plate and the HW70 plate by using crack gauges and a 15 power magnifying glass with 1/20 mm micro scales.

The fatigue crack propagation results obtained, fatigue crack growth rate, da/dN, and stress intensity factor ranges, ΔK, were plotted in the conventional manner(2), that is, log-log plots of da/dN as a function of ΔK represented in the form of

$$\frac{da}{dN} = C\,(\Delta K)^m \qquad (1)$$

to evaluate the material constants, C and m, that characterize the fatigue crack propagation behavior of hybrid members.

An effect of a slight difference of crack growth rate between SS41 and HW70 can be considered by using the Ishida's formula for an eccentrical crack in a finite plate (3) in calculating the value of K, based on the fact that the crack center shifted from the plate center as the crack grew. The eccentricity caused by the difference

of the crack growth rate, however, was small compared with the plate width, as was noted in previous report (1), such effect proved to be macroscopically negligible. The exposed fracture surface of the specimen is shown in Fig.2.

Table 1 Chemical Analysis and Mechanical Properties of Materials

Chemical Composition (Wt. %)											
	C	Si	Mn	P	S	Cu	Ni	Cr	Mo	V	B
WES-HW70	0.10	0.30	0.85	0.007	0.010	0.19	0.78	0.46	0.33	0.035	0.004
JIS-SS41	0.18	0.04	0.95	0.014	0.028	--	--	--	--	--	--

Mechanical Properties				
	Y.P.(kg/mm^2)	U.T.S.(kg/mm^2)	Elong.(%)	$_vE_{-5}$(kg·m)
WES-HW70	80	84	27	15.6
JIS-SS41	27	46	30	--

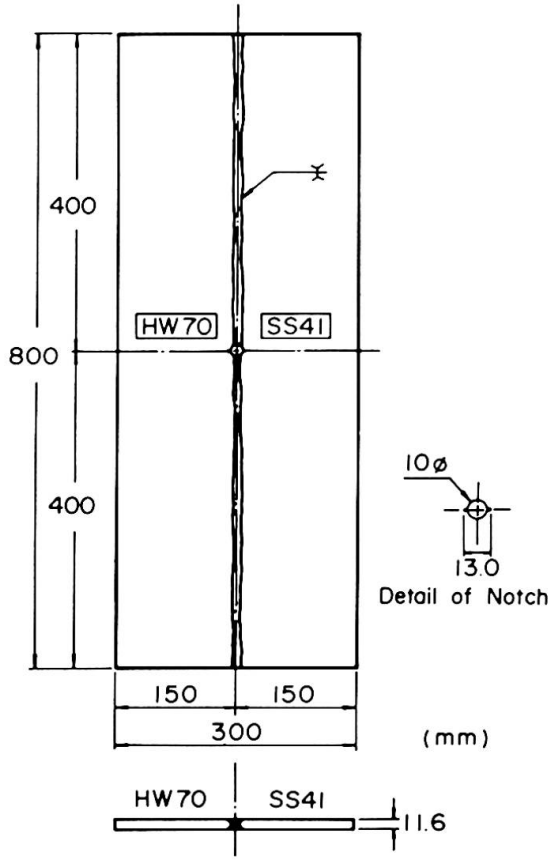

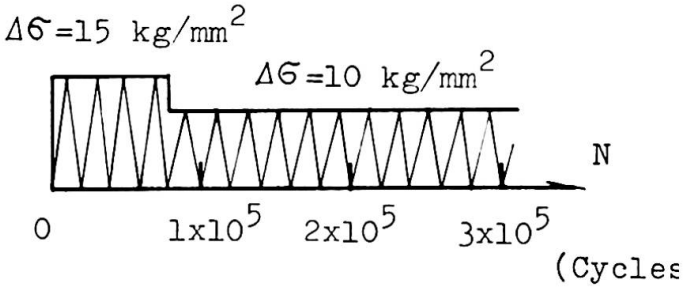

Fig.1 Configuration of Specimen and Stress Sequence

Fig.2 Exposed Fracture Surface

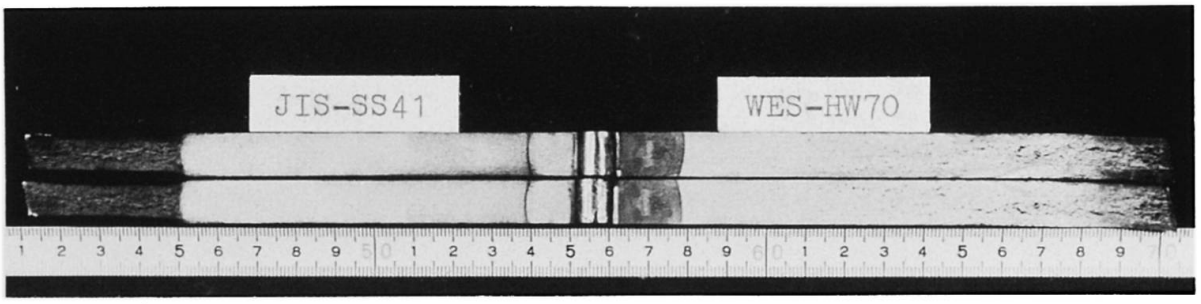

Fatigue crack growth rates, da/dN, in terms of Eq.(1) were shown in Fig.3, and the best fitted line by the method of least squares is also given in comparison with the derived crack-growth relationship given by Fisher et al.(4), a conservative upper bound for growth rates on ferrite-pearlite steels proposed by Barsom(5) and the authors' previous test results(1). The calculated material constants, C and m, were 1.2×10^{-11} and 3.6, respectively, namely the fatigue crack growth rate is numerically represented as

$$\frac{da}{dN} = 1.2\times10^{-11}\times(\Delta K)^{3.6} \qquad (2).$$

3. FATIGUE LIFE PREDICTION

To predict the fatigue lives on the previous hybrid tee-shaped specimens(1), these material constants and the value of K for a disk-like penny shaped crack in infinite body (6),

$$K = \frac{2}{\pi}\sigma\sqrt{\pi a} \quad ,$$

can be used, and the estimated S-N curves are calculated from the integrated version of Eq.(2).

The calculated S-N curves are shown in Fig.4 for various initial crack sizes, a_i, together with the test results on the hybrid tee-shaped specimens. The figure reveals that the predicted S-N curve taking the initial crack size, a_i, as 0.5 mm agrees well with the test results. This crack size of 0.5 mm is the same as the previously assumed one(1).

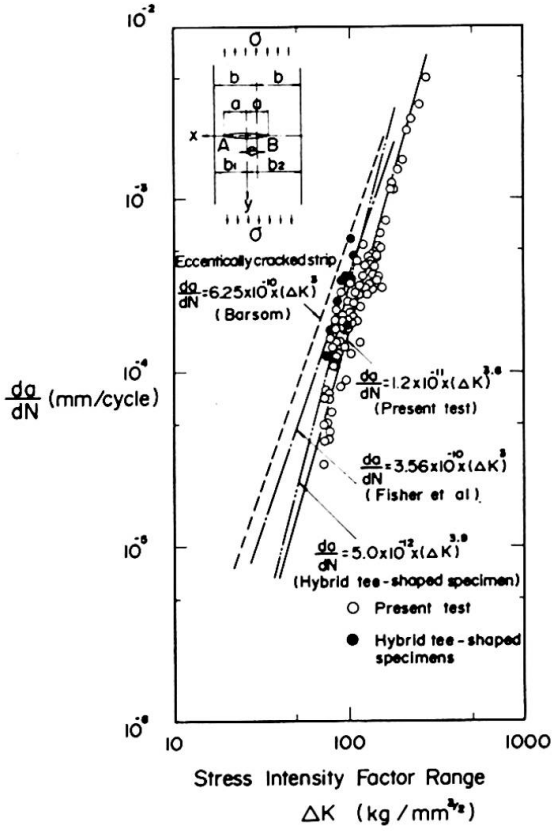

Fig.3 Summary of Fatigue Crack Growth Rate

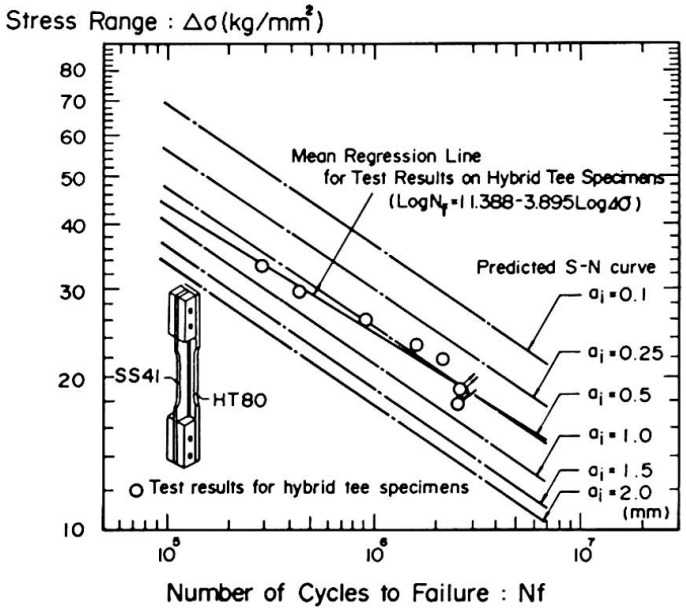

Fig.4 Comparison of Predicted S-N Curves and Previous Fatigue Test Results on Hybrid Tee-shaped Specimen(1)

4. CONCLUDING REMARK

The calculated S-N curve by using fracture mechanics, taking the initial crak size of 0.5 mm, successfully agreed well with the test results. Consequently, the fatigue life prediction method by fracture mechanics approach proved to be an effective tool for also hybrid members, if only a pertinent initial crack size can be evaluated.

REFERENCE

1) T.Yamasaki, M.Hara, Y.Kawai;Preliminary Report, IABSE, 10th Congress, 1976
2) P.C.Paris, F.Erdogan;Trans. of ASME, Series D, Vol.85, No.4, 1963
3) M.Ishida;Trans. of ASME, Series E, Vol.33, No.3, 1966
4) M.A.Hirt, J.W.Fisher;Eng. Frac. Mech., Vol.5, 1973
5) J.M.Barsom;U.S. Steel Corp., Applies Res. Lab. Rpt., 1971
6) I.N.Sneddon;Proc. Royal Soc., London, Vol.A-187, 1946

SUMMARY

A fatigue crack propagation test was conducted on a longitudinally butt welded 'WES-HW70' --'JIS-SS41' hybrid plate specimen to predict fatigue lives of hybrid members. The fatigue crack growth rates obtained were represented as a function of stress intensity factor ranges in the form of the so-called Paris' law. By using the material constants and fracture mechanics approach, the fatigue lives were successfully estimated on the hybrid tee-shaped specimens which were previously tested.

RESUME

La propagation d'une fissure due à la fatigue a été étudiée sur une plaque hybride en WES-HW70/JIS-SS41 soudée bout à bout, afin de prédire la résistance à la fatigue. Le développement de la fissure ainsi obtenue a été représenté en fonction des facteurs de concentration de contraintes, selon la loi dite de Paris. Au moyen des constantes des matériaux et de la mécanique de fissure, on a pu déterminer la résistance à la fatigue d'échantillons en forme de T qui avaient fait auparavant l'objet d'essais.

ZUSAMMENFASSUNG

Die Ausbreitung eines Ermüdungsrisses wurde an einer stumpf geschweissten hybriden Platte aus WES-HW70/JIS-SS41 untersucht, um daraus die Lebensdauer von hybriden Elementen vorhersagen zu können. Die gewonnene Rissausbreitungsgeschwindigkeit wurde in Funktion des Spannungskonzentrationfaktors nach dem sogenannten Paris'schen Gesetz dargestellt. Ausgehend von den Materialkonstanten lieferte die Bruchmechanik eine Vorhersage für die Lebensdauer von T-förmigen hybriden Proben, die vorher experimentell untersucht worden waren.

The Application of J_{IC} Fracture Criterion to the Fracture of Connections in Steel Structures

Application du critère de rupture J_{IC} au comportement à la rupture d'assemblages en construction métallique

Anwendung des Bruchkriterions J_{IC} auf das Bruchverhalten von Verbindungen im Stahlbau

HIROFUMI AOKI
Associate Professor
Yokohama National University
Yokohama, Japan

TADAO NAKAGOMI
Graduate Student
Tokyo Institute of Technology
Tokyo, Japan

1. INTRODUCTION

The criterion based on critical stress intensity factor K_{IC} is applicable to brittle fracture in low stress level, and the design procedure has been satisfactorily established on this account. While, much of our concern is now paid to the fracture in high stress level such as the case of general yielding in the section of members. One of the examples of this kind is the transition fracture of heavy members of framework at room temperature reported by Prof. Ben Kato.[1)]

As one of the nonlinear fracture mechanics, the COD criterion is introduced in the introductory report, and strain around crack tip has been related to crack opening displacement by F.M.Burdekin.[2)] The COD theory, however, reveals to be indefinite in its physical concept when applied to wider yield portion. On the other hand, comprehensible is the physical concept of J_{IC} fracture criterion[3,4)] which is the extension of the concept of energy release rate G to nonlinear region, and because J_{IC} is comparatively insensitive to the scale effect, the specimens to obtain J_{IC} may be made smaller than those for K_{IC}.

In discussing the basic applicability of J_{IC} fracture criterion, J_{IC} value of SM50B(B class) and SM58QT(C class) are obtained from the 3-point bending test at room temperature.

Bending tests are carried out for the specimens of 4 types in various stress distributions,[5)] and the fracture configurations are discussed based on J_{IC} fracture criterion.

2. COMPARISON OF J_{IC} VALUES BETWEEN SM50B AND SM58QT

2.1 Specimens and Experimental Procedure

J_{IC} values are obtained from the 3-point bending test for which specimens are made from steel plates 25mm of SM50B and SM58QT. Chemical composition, mechanical properties and Charpy values of the materials are shown in Table-1~3 respectively.

The shape of the specimens, as shown in Fig.-1, is based on ASTM E399-72 and BS DD-19. All specimens are prepared with

fatigue crack at the tip of the crack. Three kinds of crack length, 23mm, 25mm and 27mm are adopted for the specimens of SM50B. The crack length for the specimen of SM58QT is either 23mm or 25mm.

The bending test is carried out at room temperature(+20°C) and -65°C. Since it is difficult to determine the displacement δ_c experimentally to initiate crack propagation at room temperature, the crack propagation is checked by cutting the specimens in the cource of experiment after J. A. Begley and J. D. Landes.[6]

The value of J integral is obtained approximately from the following equation.

$$J = \frac{2}{Bb}\int_0^{\delta_i} Pd\delta \qquad (1)$$

where, B: Width of the specimen
b: Difference of crack length a from height W
P: Load
δ: Displacement at the loading point

2.2 Test results

Relationships between J value and increment of crack length Δa are shown in Fig.-2 which are lead by P~δ diagrams in the bending test. The results from the experiments on various crack lengths present reasonable J_{IC} values. It is recognized, therefore, that the method proposed by Begley and Landes for determining J_{IC} value should be available.

Fig.-3 shows a comparison of J~Δa relationships between SM50B and SM58QT obtained from the bending test.

In the study by J. R. Rice, et al.[7], J value is calculated for simplified P~δ relationships composed of elastic part and perfectly plastic part beyond general yielding. In this paper, P~δ relations are computed up to the general yield point by applying finite element method. After reaching the general yield point, P~δ relation is assumed as perfectly plastic. Fig.-4 shows the element division of the specimen. Calculated values of J integral are compared with the experimental results in Fig.-5.

It is confirmed that the above method for estimation of J value by calculation should be available.

It is observed in Table-4 that J_{IC} value of SM58QT is considerably smaller than that of SM50B at room temperature. Seeing that J_{IC} value of SM58QT at -65°C is larger than that of SM50B, the difference of J_{IC} values at room temperature should be adequately noted.

3. DISCUSSION CONCERNING THE FRACTURE OF TEE-JOINTS

It is emphasized in the introductory report that the welding condition free of micro cracks and steels possessing enough notch toughness should be substantial to prevent unstable brittle fracture. Further investigation should be focussed on the relations of notch toughness of material and fracture under complex stresses such as connections in steel structure.

Bending tests by using the specimens of 4 types are carried out in various stress states and conditions of test temperature. As shown in Fig.-6, the thickness of the specimens is 25mm and roller span is 280mm.

The specimen of J-type has the ratio of thickness to width 25:35 and this type is a model to expect plane stress. The ratio

Table-1 Chemical Composition (%)

Grade of Steel	C	Si	Mn	P	S	Cu	Cr	Nb	V
SM50B PL25mm	0.16	0.39	1.46	0.014	0.025	0.01	—	—	—
SM50B PL65mm	0.16	0.46	1.45	0.008	0.007	0.31	0.03	0.036	—
SM58QT PL25mm	0.12	0.27	1.11	0.012	0.007	—	0.16	—	0.03

Table-2 Mechanical Properties

Grade of Steel	Y.P.	T.S.	EL.	φ
SM50B PL25mm	41	60		73
SM50B PL65mm	39	56	38	77
SM58QT PL25mm	55	71	30	71

Y.P.: Yield Point (kgf/mm²)
T.S.: Tensile Strength (kg/mm²)
EL.: Elongation (%)
φ: Reduction of Area (%)

Table-3 Charpy Values

Grade of Steel		$_vE_0$	$_vT_{rE}$	$_vT_{rS}$
SM50B PL25mm	Surface	15.1	-6	-7
	(1/2)t	12.5	-12	-10
SM50B PL65mm	Surface	30.0	-67	-65
	(1/2)t	30.0	-52	-54
SM58QT PL25mm		24.0 *		

$_vE_0$: Absorbed energy at 0°C, but * is at -5°C (kgf.m)
$_vE_{rE}$: Energy transition tempetrature (°C)
$_vE_{rS}$: Surface transition temperature (°C)

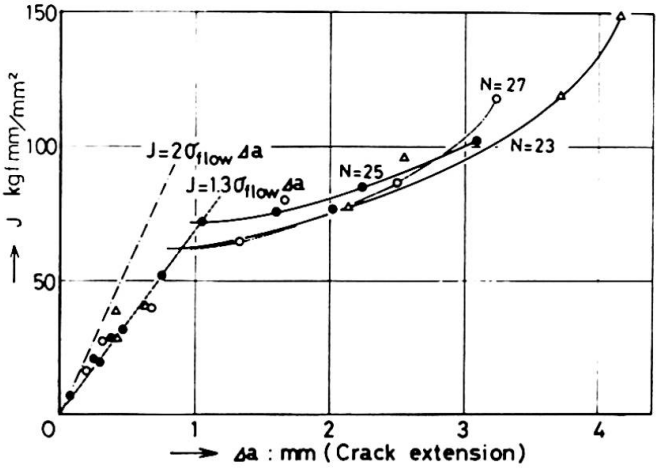

Fig.-2 Relations between J and Δa (SM50B)

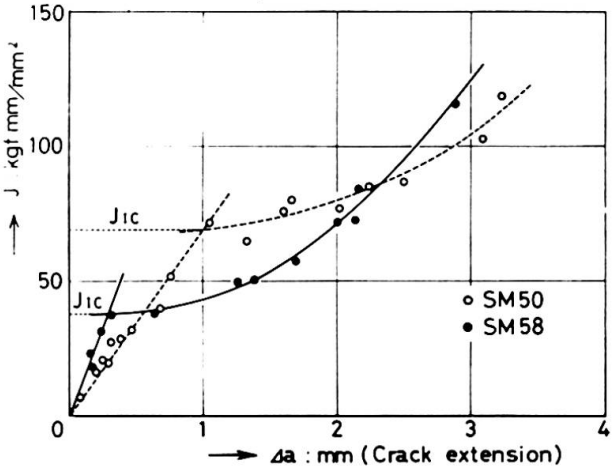

Fig.-3 A comparison of J~Δa relations between SM50B and SM58QT

Table-4 J_{IC} (kgf.mm/mm²) values

Grade of Steel	Test Temperature 15°C	-65°C
SM50B pl25	63	12.8
SM58QT PL25	43	15.1

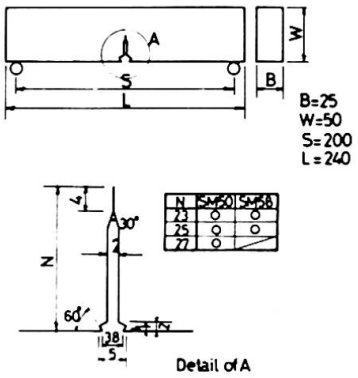

Fig.-1 Specimens for the 3-point bending test

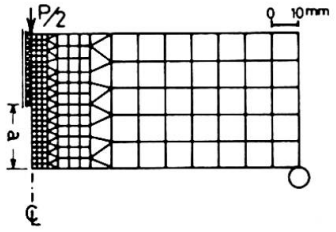

Fig.-4 Element division

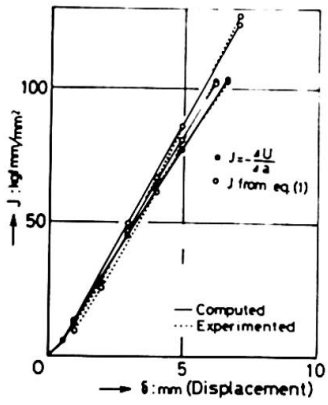

Fig.-5 Relations between J and δ

of M-type is 25:125 to expect plane strain state. B_T-type is made of steel plate 25mm with a Tee-joint where is welded. Tee flange of this type is the same dimension as M-type. The specimen of A_T-type is shaped from steel plate 65mm in order to eliminate the influence of welding. The dimension of A_T-type is same as that of B_T-type except fillet portion. The fillets of A_T and B_T-type are shown in detail in Fig.-7, respectively. The radius r at the toe of fillet in A_T-type specimen is determined to be 2mm in order to approach the same condition as the welded part in B_T-type. B_T specimen is built up by manual welding and stress relief annealing is not treated after welding. A_T and B_T-type are both pull-bend specimens.

The specimens of J-type, M-type and B_T-type are made from the steel plate which is dealt with at the preceding section. The properties of SM50B plate 65mm for A_T-type are also shown in Table-1~3. J_{IC} values for these mother metals and welded portion of the joint are summarized in Table-5.

Fig.-8 shows the relationships between the maximum bending angle θ_{max}(degree) and the test temperature T°C obtained from these bending tests.[4] It is observed in this figure that the more complex the stress state is, the smaller θ_{max} is. Especially, the specimen of B_T-type with welded joint might be the most fragile in these 4 types.

J values of the specimens are estimated by the method described at previous section. Element divisions are shown in Fig.-9.[6] J values are obtained by computing two P~δ relationships of the cases a/W=0 and a/W=2/25. Fig.-10 shows the computed results of P~δ relationships.

J_C value for each specimen which is J value at fracture of the specimen is determined by θ_{max} and P~δ curves. The ratio of J_C to J_{IC} is shown in Table-5.

This result indicates that the more complex the stress distribution of the specimen is, the smaller J_C/J_{IC} is. This ratio comes to almost unit in the case of B_T.

4. Conclusion

J_{IC} values of SM50B and SM58QT both of which are obtained from the 3-point bending test at -65°C are remarkably equal, nevertheless J_{IC} value of SM58QT is approximately 2/3 of that of SM50B at room temperature.

Experimental results from bending tests on various stress states of 4 types specimens indicate that the more complex the stress distribution is, the more fragile the joint of steel structure is. And this phenomenon can be explained by J_{IC} fracture criterion.

Finally, it should be pointed out that the independence of path in J integral is valid only under the deformation theory, and it is not directly applicable to the frames in which stress redistribution may take place significantly. J integral in this paper is introduced beyond limitation in this sence. It is necessary, therefore, to obtain more basic experimental data in order to apply J_{IC} fracture criterion in practice.

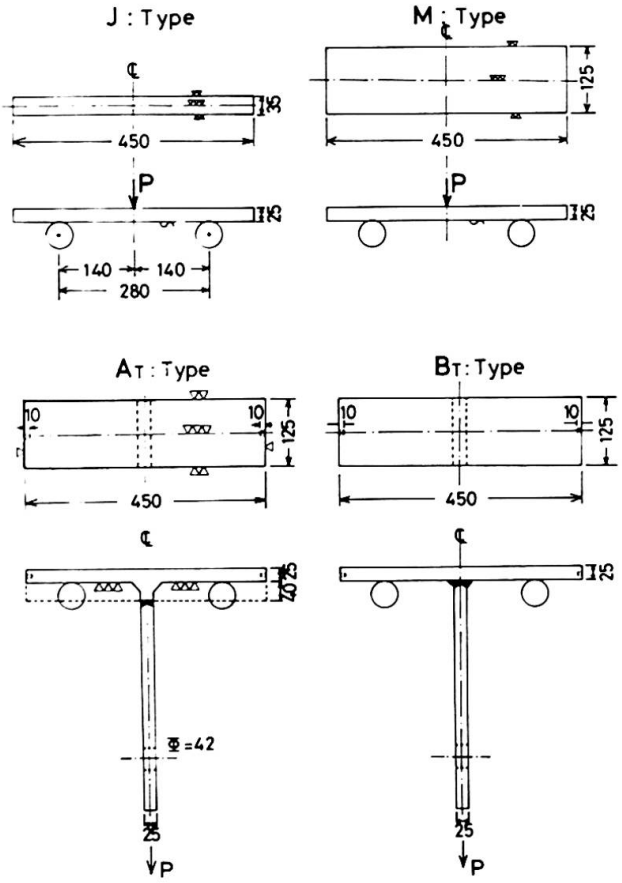

Fig.-6 Specimens of 4-types for bending tests

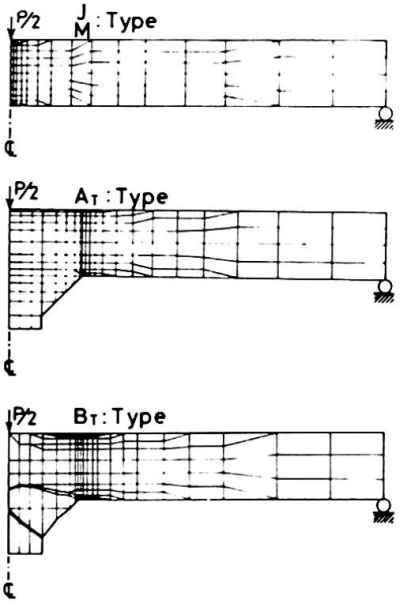

Fig.-9 Element division for 4-type specimens

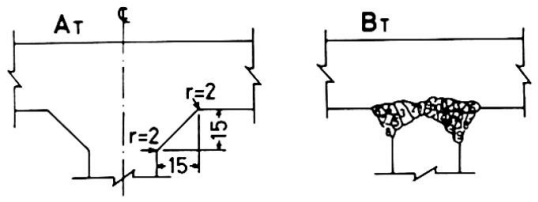

Fig.-7 Details of the fillets

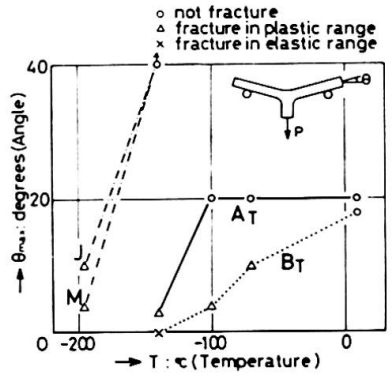

Fig.-8 Test results

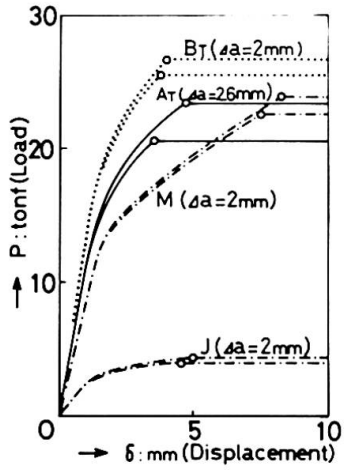

Fig.-10 Computed results

Table-5 J_C Value and the Ratio to J_{IC}

	J-type	M-type	A_T-type	B_T-type
$J_C(\frac{kgf.mm}{mm^2})$	35.46	8.42	143.11	30.38
$J_{IC}(\frac{kgf.mm}{mm^2})$	0.49	0.49	76.24	26.80
J_C/J_{IC}	72.4	17.2	1.88	1.13

5. REFERENCES

1. Kato,B.,Brittle Fracture of Heavy Steel Members,National Conf. on the Planning and Design of Tall Building,Tokyo,August,1973
2. Burdekin,F.M. and Dawes,M.G.,Practical Use of Linear Elastic and Yielding Fracture Mechanics with Particular Reference to Pressure Vessels,Conf. Practical Application of Fracture Mech. to Pressure Vessel Technology,London,May,1971
3. Rice,J.R.,A Path Independence Integral and the Approximate Analysis of Strain Concentration by Notches and Cracks,J.Appl. Mech.June,1968
4. Begley,J.A..and Landes,J.D.,The J Integral as a Fracture Criterion ,ASTM STP 513,1972
5. Fujimoto,M.,Aoki,H.,Nakagomi,T. and Hosozawa,O.,Study on Fracture of Connections in Steel Structure by Nonlinear Fracture Mechanics,Part 1, Trans. of A.I.J.No.238,Dec.1975(in Japanese)
6. Landes,J.D. and Begley,J.A., Test results from J-Integral Studies,an Attempt to Establish a J_{IC} Testing Procedure,ASTM STP 563,1974
7. Bucci,R.J.,Paris,P.C.,Landes,J.D. and Rice,J.R.,J Integral Estimation Procedure,ASTM STP 513,1972
8. Fujimoto,M.,Aoki,H.,Nakagomi,T. and Hosozawa,O.,Study on Fracture of Connections in Steel Structure by Nonlinear Fracture Mechanics,Part 2, Trans. of A.I.J.No.239,Jan.,1976(in Japanese)
9. Aoki,H.,Nakagomi,T. and Ogura,N.,Fracture and Deformation Capacity of Tee Welded Joints by Pull-bend Test,JSSC,Vol.11,No.110, Feb.,1975(in Japanese)

SUMMARY

J_{IC} values are compared between SM50B and SM58QT. Both are remarkably equal at -65° C, nevertheless J_{IC} value of SM58QT is approximately 2/3 of that of SM50B at room temperature. Bending tests on various stress states of 4-types specimens are carried out, and the experimental results indicate that the more complex the stress distribution is, the more fragile the joint of steel structure is. This phenomenon can be explained by J_{IC} fracture criterion.

RESUME

Les valeurs de J_{IC} sont comparées pour les aciers SM50B et SM58QT. Elles sont remarquablement identiques à - 65° C, bien que,à la température ambiante, la valeur J_{IC} du SM58QT ne soit que les 2/3 de celle du SM50B. Des essais de flexion sous différents états de contraintes ont été effectués sur des éprouvettes de 4 types. Les résultats expérimentaux montrent que, plus la distribution de contraintes est complexe, plus les assemblages sont fragiles. Ce phénomène peut être expliqué à l'aide du critère de rupture J_{IC}.

ZUSAMMENFASSUNG

Die J_{IC} Werte werden für die Stähle SM50B und SM58QT verglichen. Beide sind praktisch gleich bei -65° C, obwohl bei Raumtemperatur der J_{IC} Wert des SM58QT nur ungefähr 2/3 des Wertes des SM50B beträgt.Biegeversuche unter verschiedenen Spannungszuständen wurden an Proben mit 4 Ausbildungsformen durchgeführt; die experimentellen Ergebnisse haben gezeigt, dass die Gefahr eines Sprödbruches bei Stahlbauverbindungen mit der Komplexität der Spannungsverteilung zunimmt. Dieses Verhalten wird mit dem Bruchkriterium J_{IC} erklärt.

Further Studies on Composite Beams with Formed Steel Deck

Etudes complémentaires sur des poutres mixtes à platelage métallique

Weitere Untersuchungen über Verbundträger mit Stahlblechdecken

JOHN W. FISHER
Professor of Civil Engineering

JOHN A. GRANT
Research Assistant

Fritz Engineering Laboratory, Lehigh University
Bethlehem, Pennsylvania, U.S.A.

After publication of our paper in the Preliminary Report, Tenth Congress IABSE (1), additional tests were undertaken on composite beams with 3 in. (76 mm) formed steel deck with a w/h ratio equal or greater than 2.0 In addition, it was desirable to provide further experimental data on shear connectors with an increased embedment length above the rib. In the study reported in Ref. 1, most stud shear connectors were embedded 1½ in. (38 mm) above the rib (H - h). In the additional beam tests, all connectors were embedded 2 in. (50.8 mm) above the rib in order to optimize the shear connector resistance. The rib geometry provided w/h ratios of 2 and 2.42.

As a result of the additional beam tests, the shear connector resistance was re-evaluated and a slight modification suggested by Lim (2) was introduced into Eq. 2 of the preliminary report. It was found that replacing the coefficient 0.6 with $0.85/\sqrt{N}$ provided a better fit to the test data with single connectors in a rib, as well as providing for more than two connectors in a rib. This results in the expression:

$$Q_{rib} = \frac{0.85}{\sqrt{N}} \cdot \frac{H - h}{h} \cdot \frac{w}{h} \cdot Q_{sol} \leq Q_{sol} \qquad (1)$$

where N = number of shear connectors placed in a rib. The parameters w, h and H were defined previously (w = average rib width, h = height of rib, H = height of stud shear connector) and Q_{sol} is the connector strength in a solid slab.

Figure 1 shows the 56 beam tests results summarized in Fig. 4 of Ref. 1 as well as 19 additional beam tests including one test with three connectors per rib. The plot shows that Eq. 1 provides a good estimate of flexural capacity for 1, 2 or 3 connectors in a rib. Pushoff tests summarized in Ref. 3 indicate the same type of change in connector capacity with varying numbers of shear connectors in a rib. Equation 1 provides the same connector capacity as Eq. 2 in the preliminary report when two connectors are placed in a rib. For a single connector a higher capacity results which approaches the solid slab value for longer embeddment lengths.

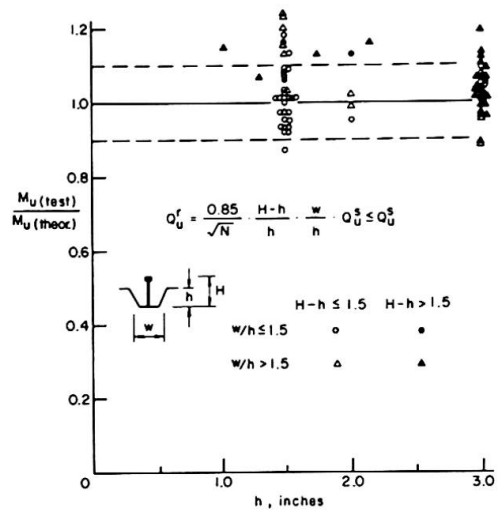

Fig. 1

In the Preliminary Report, Eq. 4 was incorrectly shown. It was intended to be expressed as:

$$I_{eff} = I_s + \sqrt{\frac{V'h}{Vh}} (I_{tr} - I_s) \quad (2)$$

The shear connection ratio was missing its exponent in the Preliminary Report.

All additional tests verified the applicability of Eqs. 1 and 2 to composite beams with formed steel deck, including deck with larger w/h ratios.

REFERENCES

1. Grant, J. A., Fisher, J. W. and Slutter, R. G., High Strength Steel Composite Beams with Formed Steel Deck, Preliminary Report, Tenth Congress, IABSE, Tokyo, 1976.
2. Lim, L. C., Private Correspondence, April 28, 1976.
3. Iyengar, S. H. and Zils, J. J., Composite Floor System for Sears Tower, AISC Engineering Journal, American Institute of Steel Construction, Vol. 10, No. 3, 1973.

SUMMARY

Additional tests on composite beams with formed steel deck verified that the w/h ratio could be extended beyond 2. A modification to the expression developed for shear connection capacity was found to provide for differing numbers of shear connectors installed in a rib.

RESUME

Des essais complémentaires sur des poutres mixtes avec platelage métallique ont montré que le rapport w/h (largeur de la nervure/hauteur de la nervure) peut être étendu au-delà de 2. Une modification de l'expression développée pour la résistance des connecteurs a permis de tenir compte du nombre de connecteurs par nervure.

ZUSAMMENFASSUNG

Zusätzliche Versuche an Verbundträgern mit Stahlblechdecken zeigten, dass das w/h Verhältnis (Rippenbreite/Rippenhöhe) über 2 hinaus vergrössert werden darf. Eine Erweiterung des Ausdruckes für die Dübeltragfähigkeit, die die Anzahl der Dübel pro Rippe berücksichtigt, ist gefunden worden.